Available online at www.sciencedirect.com

jmr&t Journal of Materials Research and Technology

journal homepage: www.elsevier.com/locate/jmrt

Heat treatments of 17-4 PH SS processed by SLM to improve its strength and biocompatibility in biomedical applications

C. Garcia-Cabezon [a,b,*], C. García Hernández [a,b], M.A. Castro-Sastre [c], A.I. Fernandez-Abia [c], M.L. Rodriguez-Mendez [b,d], F. Martin-Pedrosa [a,b]

[a] Materials Engineering, E.I.I., Universidad de Valladolid Valladolid, 47011, Spain
[b] BioecoUVA Research Institute, Universidad de Valladolid Valladolid, 47011, Spain
[c] Department of Mechanical, Informatics and Aerospace Engineering, Universidad de León, Campus de Vegazana León, 24071, Spain
[d] UVASENS, E.I.I., Universidad de Valladolid Valladolid, 47011, Spain

ARTICLE INFO

Article history:
Received 17 April 2023
Accepted 12 August 2023
Available online 17 August 2023

Keywords:
17-4 PH SS
Biomaterial
Corrosion
Selective laser melting

ABSTRACT

This research investigates the impact of heat treatment on the microstructure, hardness, and corrosion resistance of 17-4 PH SS (stainless steel) processed by Selective Laser Manufacturing (SLM) in Phosphate Buffer Solution (PBS) and compared to its commercial wrought counterparts. The SLM process produced a segregated microstructure with significant variations in composition and phases. Post-process heat treatment resulted in a uniform and reproducible microstructure in the SLM samples with a significant improvement in corrosion resistance in the solubilised samples and a remarkable hardening in the solubilised and aged samples. Additionally, heat-treated SLM samples showed no relevant release of metallic elements to PBS electrolyte after 75 days of immersion, indicating its potential use as a biomaterial. The study concludes that the manufacturing process used to produce SS have a significant impact on its properties, moreover, post-build treatment improve microstructure providing uniformity which positively impact in the corrosion resistance. The electrochemical results also suggest that, after homogenization, the additively produced 17-4 PH SS shows a better behaviour in biological environment than the wrought 17-4 PH SS.

1. Introduction

Research in biomaterials and medical implants, surgical devices, and tools is becoming increasingly important as they are an essential element in improving human health and quality of life. Materials intended for medical use must meet all clinical, mechanical, manufacturing, and economic requirements. In the field of medicine, the most commonly used materials are natural and synthetic polymers, ceramics and metals. Among the metals, titanium alloys, cobalt-chromium alloys, and stainless steel (SS) are the most commonly used ones [1]. Despite the large number of

* Corresponding author. Materials Engineering, E.I.I., Universidad de Valladolid Valladolid, 47011, Spain.
E-mail address: crigar@uva.es (C. Garcia-Cabezon).
https://doi.org/10.1016/j.jmrt.2023.08.104

biomaterials available, the selection of materials for the medical field is a complicated task, where the choice of which depends primarily on the application. In the case of implants, devices, and surgical tools, metallic alloys are the most suitable option due to their good mechanical properties in terms of strength, wear, and corrosion resistance [2]. Another expected property is its biocompatibility, a term that ISO 10993-1:2018 defines as the "ability of a medical device or material to function with an appropriate host response in a specific application". Considering all of these aspects, despite the large number of compatible metallic alloys with the medical industry [3–5] SSs are good candidates due to their excellent mechanical properties [6–8], as well as their high corrosion resistance. Additionally, some SS alloys, such as 316, 316L, 304 and 17-4 PH, have additional properties that make them suitable for surgical applications, such as good biocompatibility, low risk of allergic reactions, ability to withstand intense sterilization processes used in the medical industry. Among the SSs used, 17-4 PH SS has gained significant attention due to its good combination of high strength, high toughness, and good corrosion resistance [9]. For these reasons, it is being used for medical and computer applications, in the chemical industry and for equipment in the automotive and aerospace fields [10–13]. This material is an alloy of chromium, nickel and copper, which can be precipitation hardenable. Furthermore, several studies have shown promising results in terms of its biocompatibility [14] and mechanical properties for applications in the medical field.

Traditionally, the processing of 17-4 PH SS for medical devices has been done through forging and machining, although MIM technology offers a more suitable and affordable alternative [15]. Various research studies using MIM technology have confirmed its suitability for the manufacture of medical components due to the properties of the resulting parts, relatively complex component fabrication in very large quantities, as well as an economical alternative [16–18]. There are several published works on medical devices made from MIM, for example, the company Indo-MIM produced a set of retractor blades and ring used in a spinal surgery procedure using 17-4 PH SS by MIM. Furthermore, the Metal Powder Industries Federation (MPIF) used blocks of this metal as an advanced instrument for knee replacement surgery to produce medical forceps. In addition, it has been validated in some research works for the manufacture of orthodontic brackets [9,15].

Despite these advantages of MIM technology, additive manufacturing (AM) is currently the only technique that can produce more complex and customized parts. The importance of customization in the medical device industry is mainly because each patient has their own individual anatomy. In addition, AM have emerged as promising manufacturing technique because they offer a reduction in operator error and increased repeatability, speed, cost-effectiveness, and reduction of material waste compared to conventional techniques [19]. According to the standards established by the International Organization for Standardization (ISO) and the American Society for Testing and Materials (ASTM), AM can be divided into seven categories. Each manufacturing technology is more suitable for a specific material and has advantages and disadvantages [20], and therefore the choice of both, technology and material, depends on the specific application to be carried out. In particular, SLM has been optimized and studied according to these requirements to work with biocompatible materials. It has specifically demonstrated great potential for the manufacturing of dental prostheses using two biocompatible metal alloys, Ti–6Al–4V and Co–Cr–Mo rich precipitates [21]. In this work, Ben et al. indicate that this technique provides the necessary requirements in terms of mechanical and chemical properties of the manufactured product, and the process guarantees high precision, although with high surface roughness.

On the other hand, 17-4 PH SS has also been processed by SLM [22–26]. Numerous studies have reported findings that show superior mechanical characteristics [27] and greater resistance corrosion in different corrosive environments such as chloride solution [28], marine, industrial, freshwater, oil and vapor environments [29], as well as in media containing sodium chloride and sulfuric acid media [22]. The use of SLM technology is mainly focused on improving porosity through different manufacturing strategies, such as the hexagonal scanning [26], double scanning, and subjecting samples to a HIP treatment [24] to reduce porosity and enhance corrosion resistance in various environments. In the study by Lashgari et al., it was found that in the phosphate-buffered saline (PBS) solution, the corrosion rate of samples manufactured using the hexagonal scanning pattern was generally lower than those manufactured using the concentric pattern due to reduced porosity. It has also been found in other studies that these improvements in mechanical properties and corrosion resistance are kept when compared to traditional manufacturing processes [22,30]. However, to date, no studies have been conducted in biological media that accurately simulate the physiological conditions of the human body.

Despite the advantages of AM over other technologies and the potential of 17-4 PH SS for use in medical applications, further exploration is still needed as both the material and technology still present disadvantages, and therefore, research must continue. Among the disadvantages:

1. SLM manufacturing can be expensive and requires specialized equipment and detailed planning, support for mass production, and part size are limited [31].
2. The microstructure, mechanical properties, and surface finish are affected by SLM printing parameters, requiring careful optimization to ensure the quality of the final product [32].
3. Metal AM has a limitation in the application of additively manufactured parts in different industries (biomedical engineering, aerospace, and household appliances) due to its lack of uniformity and high surface roughness [33].
4. Biocompatibility can be limited due to the presence of certain alloy elements such as nickel and cobalt [15]. The release of these and other metals can result in adverse effects including toxicity, carcinogenicity, and allergy [34,35].

Therefore, it is important to focus efforts on improving these aspects related to both technique and material, since the processing of 17-4 PH through SLM can affect its mechanical and corrosion properties, which can have

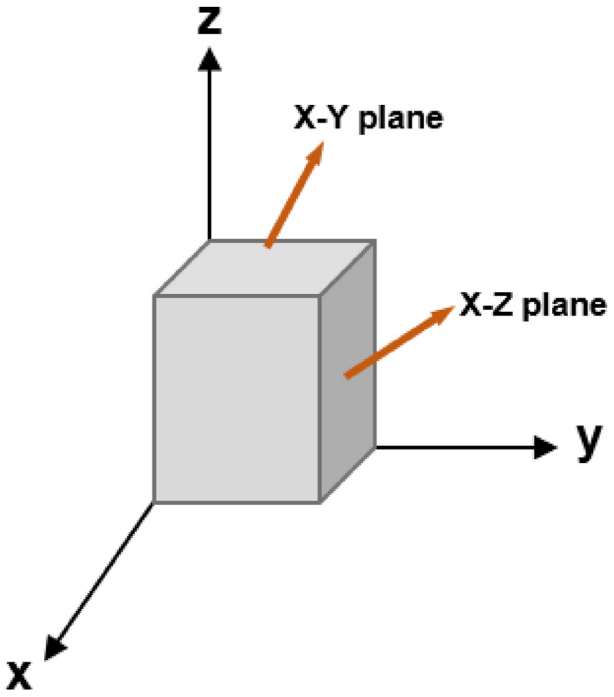

Fig. 1 – X–Y and X–Z planes of the specimens.

implications for its biocompatibility. In fact, there are several studies that have focused on optimizing processing parameters [22] and post-processing to improve the surface quality of the final part, such as heat treatments [36,37] and coatings [38,39].

Despite the interest in 17-4 PH SS as a biocompatible material, as well as the benefits of SLM technology for processing such material and for medical applications, there is still a scarcity of contributions in the material-technology-medical application combination. Guided by the aforementioned issues and motivated to contribute to an improvement in the mechanical and biocompatibility properties of 17-4 PH SS, the objective of this article focuses on understanding and addressing the corrosion of such processed material through SLM and conventional processes (Wrought) using PBS (Phosphate-Buffered Saline) as a medium, commonly used to simulate physiological conditions in the human body. Inductively Coupled Plasma Optical Emission spectroscopy ICP-OES tests were also conducted to determine which metals were released in the corrosion process, as well as the amount released. Some pieces were immersed in the same medium for 75 days and analysed using inductively coupled plasma (ICP) with optical emission spectroscopy. In addition, since it has been shown that heat treatments provide additional benefits in terms of microstructure, mechanical properties, surface finish, and corrosion resistance, an annealing and precipitation hardening (age hardening) to the material was applied.

2. Methods

2.1. Samples and characterization

In this study, the behaviour of 17-4 PH SS additively manufactured using SLM followed by heat treatment is compared to its as-built SLM and to its commercial wrought counterpart. For this purpose, the SLM samples were X–Y planes, perpendicular to the built direction, and X–Z planes, parallel to the built direction (Fig. 1). The chemical composition of the 17-4 PH SS powder used for SLM fabrication and of the wrought samples are shown in Table 1 and in a previous work it has been published a detailed description of the fabrication process [22]. The main processing parameters are indicated in Table 2.

The SLM 17-4 PH SS samples were hardened by solubilised and ageing (precipitation hardening). Solution annealing temperature was conducted at high temperature (1050 °C) for 1h followed by quenching in oil and subsequent aging for 5h at 550 °C followed by cooling in the air. In the case of the commercial wrought sample, the heat treatment described before has been applied to the material during its manufacturing process.

Microstructural characterization was carried out using optical microscopy (OLYMPUS BX53 M) and scanning electron microscopy with energy dispersive X-ray spectroscopy (SEM/EDS) (QUANTA 200F, FEI). Etching of samples was carried out using Vilella's reagent and oxalic acid for the electrochemical etching. Phase analysis were made using X-ray difraction (XRD) (Bruker Discover D8) to obtain the patterns of the samples. Thin sections were prepared from the sample oriented parallel to the build direction. These foils were observed in a high-resolution Bruker TEM TALOS 200FX employing an EDAX EDS (X-ray) attachment. Moreover, after carrying out the corrosion assays, the specimens were observed by optical microscopy to determine the influence of them on the 17-4 PH samples surfaces.

Table 2 – Main processing parameters used for SLM samples.

Parameter	Value
Laser power (W)	38
Scanning speed (mm/s)	140
Layer thickness (μm)	30
Hatch spacing (μm)	70
Scanning strategy	Hexagons

Table 1 – Chemical composition of the SLM and wrought 17-4 PH SS samples.

Elements	%C	%Cr	%Ni	%Mo	%Mn	%Si	%Cu	%Nb	%N	%S	%Al	%Fe
Wrought	0.032	15.70	4.30	0.15	0.61	0.27	3.13	0.255	0.004	0.0005	0.005	Bal.
SLM powder	0.038	16.93	4.17	–	0.58	0.62	3.56	0.21	0.072	0.005	–	Bal.

2.2. *Mechanical characterization: micro and macrohardness*

Hardness measurements were carried out to determine Rockwell-C using a Centaur RB2 macrohardness test equipment according to ISO 6507–1. Additionally, due to the results of the macrohardness test can be influenced by the porosity of the SLM samples, microhardness test was also performed applying 100 g load during 30 s using a Matsuzawa MXT70 microhardness test equipment. For each hardness test, ten measurements were taken in different locations of the top surface of the 17-4 PH SS samples and means and standard deviations of the test were calculated.

2.3. *Corrosion behaviour*

Firstly, the 17-4 PH SS samples were prepared for the corrosion assays. For this purpose, all specimens were wet ground with SiC abrasive papers and polished with 1 μm diamond aqueous suspension Then, potentiodynamic polarization (PDP), open circuit potential (OCP) and impedance spectroscopy (EIS) have been carried out in order to study the corrosion behaviour of the samples using a potentiostat 273A EG&G PAR and a Solartron SI 1260 impedance analyzer. Electrochemical measurements were performed using a three-electrode conventional cell with the 17-4 PH SS samples as the working electrodes (1 cm^2 area of the sample was exposed), graphite as the counter electrode and a saturated calomel electrode (SCE) as the reference electrode. Electrolyte solution of phosphate-buffered saline (PBS) at 37 °C was used for all the electrochemical test to simulate severe corrosion conditions and in deoxygenated conditions (purged with nitrogen). Firstly, samples were left under OCP until the corrosion potential was constant (generally, ±10 mV/min or less) over long periods of time (1 h) indicating that the system may be stable enough, thermodynamically, which is needed for the subsequent analysis methods. Moreover, OCP values gives important information about the tendency of the metal to corrode, being a negative OCP value indicative of an electrode more likely to corrode from the electrolyte than a positive OCP value (more "noble"). After the OCP analyses, potentiodynamic polarization was carried out in order to study the passivation behaviour of the samples following the ASTM G5-87 [40]. Then, the sample potential was held at −0.25 V vs. OCP to acquire complete PDP curves at scan rates of 0.833 mV·s−1, from −0.25 V vs. OCP to 1.25 V vs. SCE. The values for the polarization resistance (R_p), potential (E_{corr}) and corrosion current density (I_{corr}) were obtained by extrapolating the Tafel slope of the polarization curves. Finally, electrochemical impedance spectroscopy (EIS) measurements were performed in potentiostatic mode at OCP in the frequency range from 10 MHz to 1 Hz. Impedance spectra were fitted with aid of the Zview2 software and equivalent circuit fitting was performed using CorrView software.

Moreover, to study the corrosion behaviour of the samples after immersion in PBS, the wrought and SLM samples (X–Z plane) were immersed in the electrolyte at 37 °C for 75 days keeping the ratio solution volume to sample surface area constant. The inductively coupled plasma-mass spectrometer

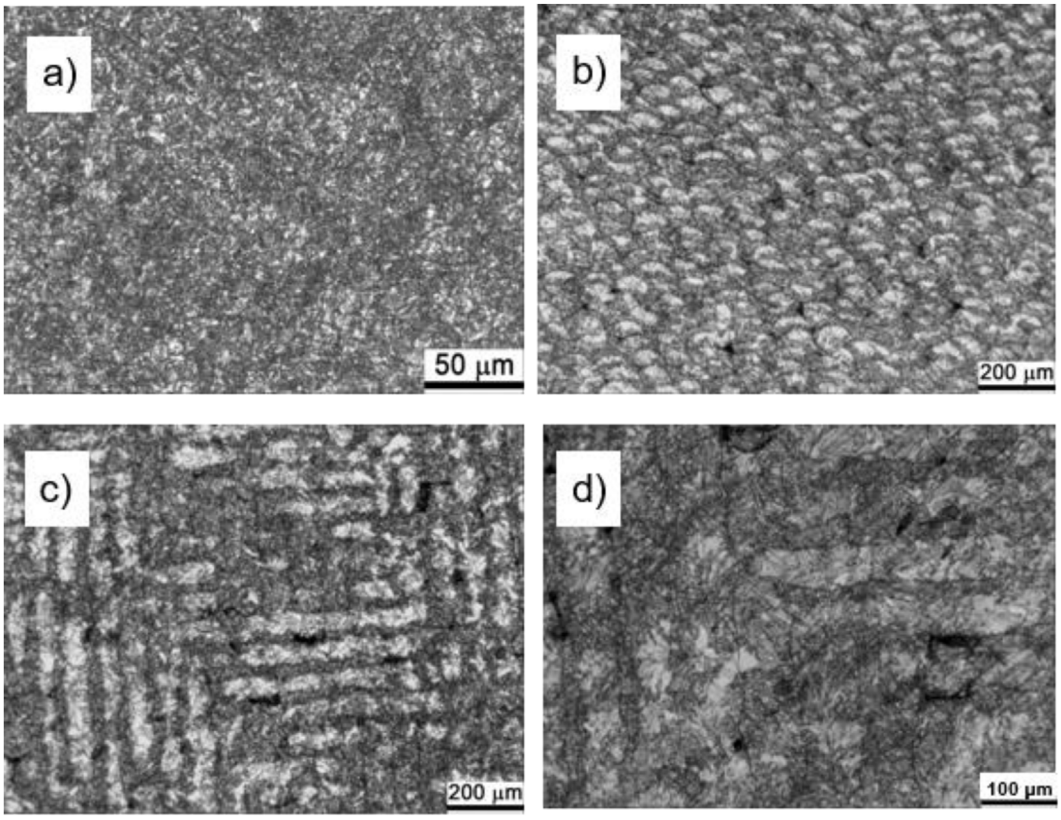

Fig. 2 – Microstructure of a) wrought 17-4 PH SS, b) SLM 17-4 PH SS (X–Z plane), c) SLM 17-4 PH SS (X–Y plane), d) microsegregation observed in SLM 17-4 PH SS (X–Y plane).

(ICP-MS) (PerkinElmer Optima 2000DV) was employed to measure the concentrations of various metal ions (Fe, Cr, Ni, Cu and/or Mo, among others) that might be released into the electrolyte. A PBS solution without a specimen was used for the blank. After the immersion period, samples were electrochemically tested using OCP and PDP and the microstructure was observed by optical microscope.

For all electrochemical tests, the measurements were repeated at least 3 times to ensure reproducibility and the average value is considered for analysis using Origin Lab Pro Software. All the presented current densities are normalized to the geometric area of the working electrode.

2.4. *Cytocompatibility tests*

In vitro experiments were performed to evaluate the biocompatibility of the samples for study the influence of manufacturing process. MC3T3-E1 mouse preosteoblasts were cultured in α-MEM with nucleosides without ascorbic acid with 10% fetal bovine serum, at 37 °C and 5% CO_2. These cells were trypsinized and seeded on 24-well plates at a density of 10,000 cells/cm^2. They were left unaltered for attachment in complete growth medium at 37 °C and 5% CO_2 for 2 h. According to the ISO10993-5 [41] the samples (wrought and SLM) were placed on the cell layer, so the material was directly in contact with the cells. After 1 and 3 days, cell viability (LIVE/DEAD assay) and metabolic activity (AlamarBlue assay) tests were performed as recommended by the manufacturer, after removing the 17-4 PH SS samples from the cells. All the experiments were performed in triplicate.

Images of LIVE/DEAD assay were taken with a Nikon Eclipse Ti-E coupled to a Nikon DS-2MBWc digital camera using the NIS-Elements Advanced Research software which allowed the automatic imaging of almost the full well surface for quantitative determination of cell viability. On the other hand, AlamarBlue reduction was measured in a fluorescence plate reader. In both cases, a positive control, (i.e. cells not in contact with samples) were used for normalization.

Table 3 – Results of porosity for SLM specimens.

	Porosity (%)	Circularity	Pore size (μm^2)
SLM (X–Y plane)	0.8	0.928 ± 0.001	32.8 ± 8.74
SLM (X–Z plane)	0.5	0.803 ± 0.011	68.5 ± 8.19

3. Results and discussion

3.1. *Microstructural characterization*

Fig. 2 shows the relevant microstructural differences for 17-4 PH SS in wrought form and its counterpart fabricated by SLM in "as-built" condition. The microstructure of wrought 17-4 PH SS, Fig. 2a, was primarily a martensite matrix, with a relatively fine prior austenite (grain size, G = 8) and later with small areas of retained austenite. No evidence delta phase islands have been observed in these micrographs. This is consistent with the literature for this alloy in the solubilised and age-hardened condition [42,43]. The microstructure of SLM 17-4 PH SS was clearly more heterogeneous with important differences between the perpendicular and parallel planes to the building direction. Columnar grains growing along the built section were observed caused by the temperature gradient in the melt pool (Fig. 2b), and, moreover, the overlapping hemispherical melt pools are clearly visible (Fig. 2c) in the perpendicular orientation (X–Y plane). In addition, the high cooling rate of SLM process have originated some dendritic segregation observed across the melt pools (Fig. 2d). The samples obtained by SLM are generally free of defects, although they occasionally might show small pores and some non-metallic inclusions [22]. The results of porosity determined by image analysis obtained in SLM specimens are shown in Table 3.

The mentioned above microstructures lead to differences in the mechanical and corrosion properties. For this purpose, post-processing heat treatment were performed in as-built SLM samples to achieve a uniform and reproducible microstructure. Thus, the microstructures of "solubilised" and "solubilised and aged" are reported in Fig. 3a and b, respectively. As can be observed the microstructure appears to be homogeneous with no trace of the melt pools and scan tracks. Furthermore, the difference between X–Y plane and X–Z plane become less important after the solubilisation treatment. Moreover, it was found that the optical microstructure was similar after aging heat treatment.

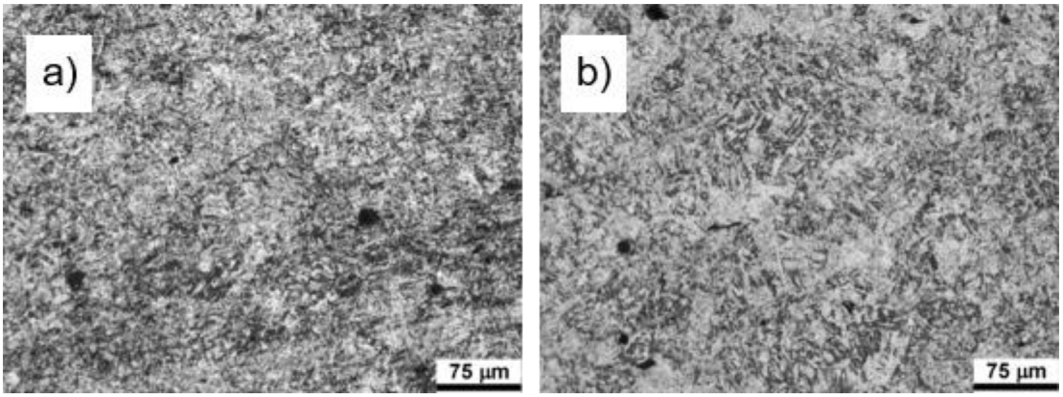

Fig. 3 – Microstructure of the 17-4 PH SS after heat treatment. a) Solubilised and b) Solubilised and aged.

The XRD spectra of the wrought steel and the SLM parts at different conditions are shown in Fig. 4. As it can be seen, the most important peaks correspond to bcc phase which could be either martensite or ferrite. Considering the low concentration of carbon in 17-4 PH SS, the expansion along the c axis is quite negligible which makes it difficult to distinguish the ferrite from the martensite based on the XRD patterns [44,45].

In the case of wrought sample, the results of the optical microstructure and the XRD pattern seem to be consistent, and they show the presence of martensite whereas in the SLM sample in "as built" condition the bcc phase could be ferrite delta or martensite. This contradiction is clear in the literature [42] and the ratio of Cr_{eq}/Ni_{eq} plays a crucial role in the solidification mechanism of SSs [46]. For a high ratio Cr_{eq}/Ni_{eq}, the high heating and cooling rates do not allow austenite formation, so initial delta ferrite cannot be transformed whereas, in this case, because of the low Cr_{eq}/Ni_{eq} ratio, the transformation of delta ferrite to austenite is allowed and, finally, austenite is transformed to martensite during cooling. In this case, the presence of nitrogen leads to lower the ratio Cr_{eq}/Ni_{eq} and, therefore, the austenitic is formed, and afterwards, transformed to martensite. Finally, the austenite transformed to martensite, which is the dominant phase at room temperature,was confirmed by the sub-sequent hardness measurements. The analysis of the XRD spectra confirmed the presence of retained austenite and some Nb–Cr precipitates in both the as-built SLM and the wrought steel.

After the solubilisation heat treatment at 1050 °C, the XRD spectrum only revealed martensite peaks and no retained austenite appeared. The high amount of retained austenite in the as-built condition could be caused by microsegregation that it is originated during additive manufacturing and it may lead to the fcc phase enriched in austenite and stabilizers (as nitrogen), resulting in a decrease in the start temperature of the martensite transformation (Ms) and, therefore, to a not complete martensite transformation. In addition, the XRD analysis of the samples subjected to the homogenization treatment showed that effectively the treatment suppresses the retention of austenite. Furthermore, there were no evidence of precipitates in the solubilised sample.

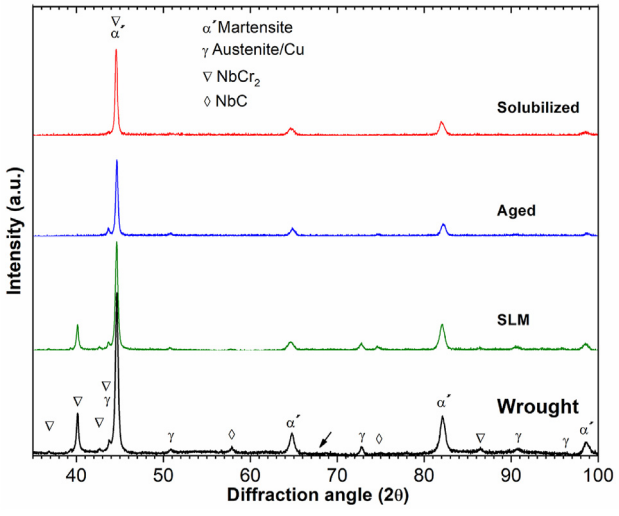

Fig. 4 – XRD spectra of the wrought and the SLM 17-4 PH specimens.

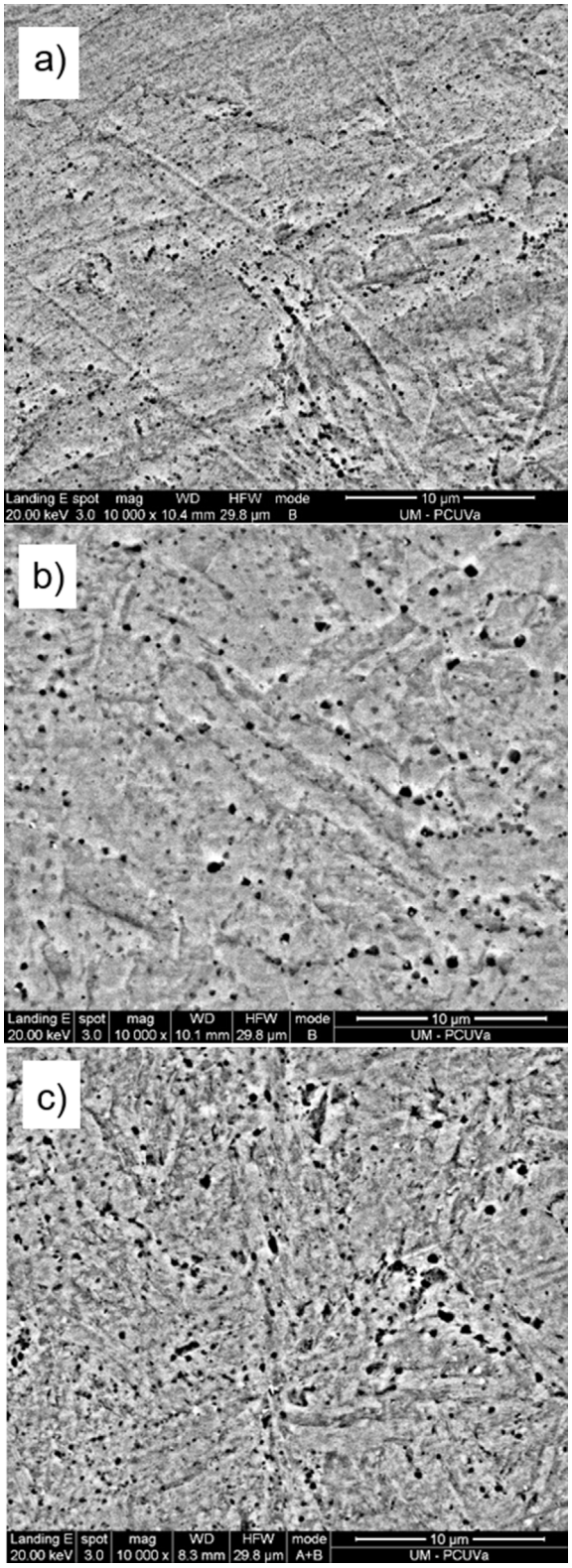

Fig. 5 – SEM images of the microstructures of the SLM 17-4 PH SS. a) In the as-built condition, b) Solubilised and c) Solubilised and aged.

The XRD spectra of the solubilised and aged sample exhibited an increase in the volume fraction of the retained austenite and the precipitates in the martensite matrix. As seen in Fig. 4, the intensity of γ (111) peak in the aged sample is higher than the obtained for the solubilised sample, indicating the formation of reverse austenite. The formation of reversed austenite was found to have a relationship with the precipitation of Cr–Mo–Nb phases because the adjacent surroundings of Cr and Mo elements become enriched of Ni, which promotes the formation of austenite during ageing [47]. Therefore, it is well known that aging in 17-4 PH SS results in the precipitation of the coherent Cu-enriched particles in the bcc matrix. Furthermore, the diffusion of Cu atoms during aging to form precipitates diminishes the martensite final temperature, facilitating the formation of reversed austenite [48,49].

Fig. 5(a–c) shows the SEM microstructures of the AM 17-4 PH specimens under different treatment conditions. The microstructure of the as-built sample showed individual melt pools (Fig. 5a) with a dendritic-cellular solidification structure with some Nb-rich precipitates (dark). Fig. 5b shows the microstructure of the solubilised sample where a homogeneous martensitic microstructure is observed, and the micro-segregation has been eliminated as well as the amount of precipitates has been reduced. This result demonstrates that a post-built thermal processing lead to a more uniform microstructure since the temperature and hold time homogenize the microchemistry and dissolve the majority of the precipitates. The micrograph of the solubilised and aged sample is shown in Fig. 5c. In comparison with the "as-built" and solubilised sample, in this sample the precipitation was increased and EDS analysis confirmed an increase in Nb and Cr content (dark areas) and that the niobium precipitates were enlarged in aged specimens. However, as the precipitates were very fine it was quite difficult to analysis them, in fact, this aspect has already been reported in the literature [37]. Finally, Cu-rich precipitates were not observed in any of the analysed samples

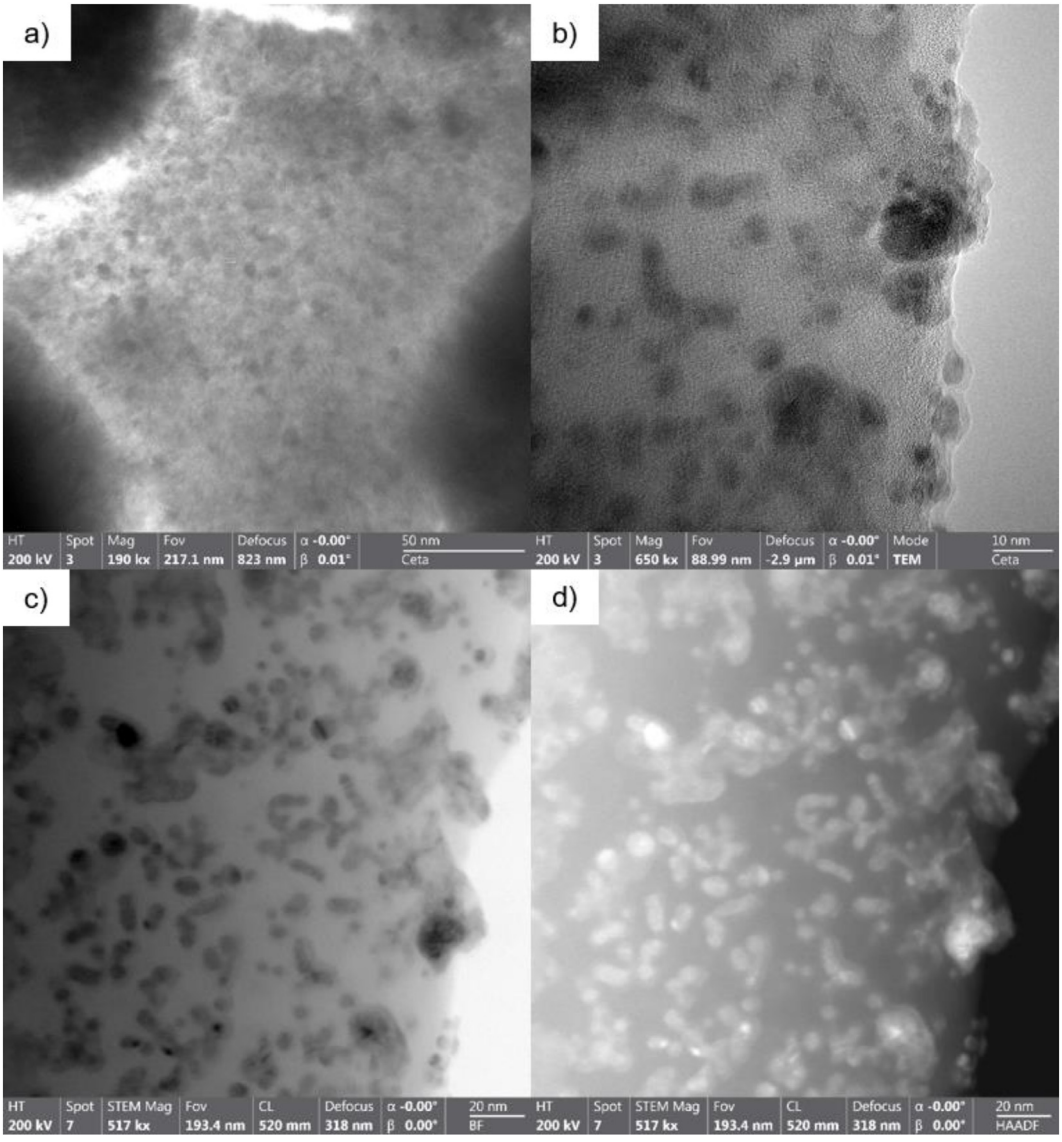

Fig. 6 – TEM images of the microstructures of the aged SLM 17-4 PH SS. a) Dark field showing cellular structure, b) dark field image showing precipitates c) bright field image showing precipitates and d) high resolution image of precipitates.

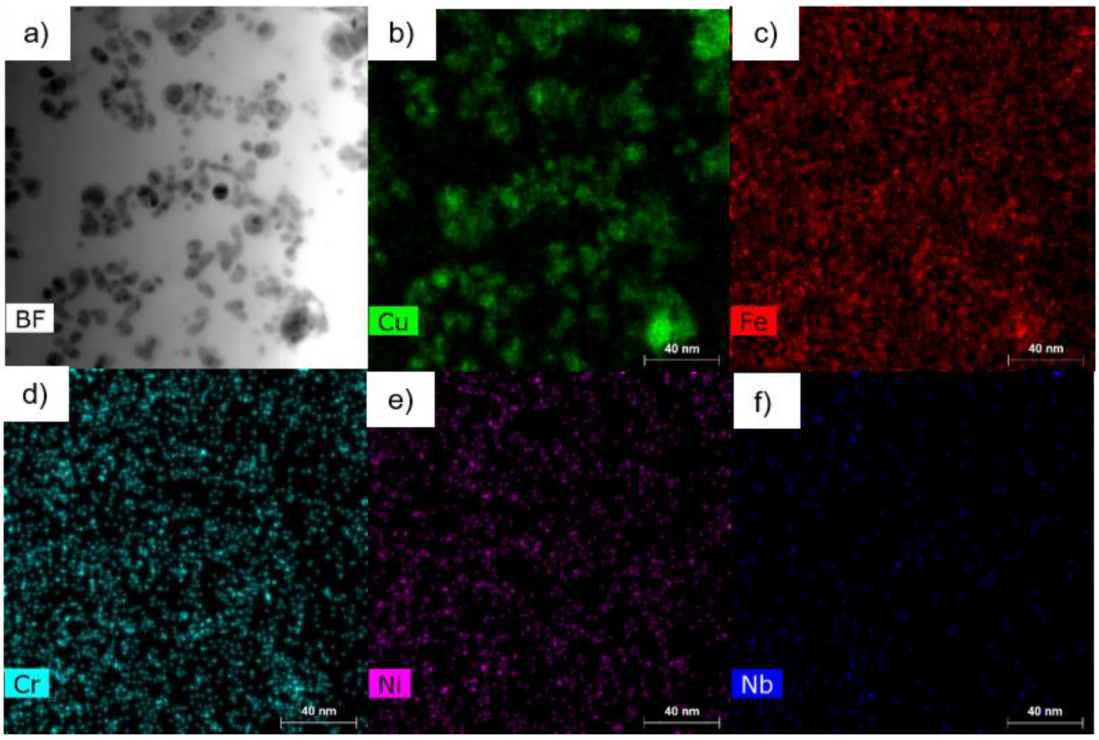

Fig. 7 – Systematic analysis for Cu precipitates. a) Brigh field image, b) X-ray map of Cu, c) X-ray map of Fe, d) X-ray map of Cr, e) X-ray map of Ni and f) X-ray map of Nb.

which was evident since their nanometric size would require a TEM microscopy analysis [36,50].

The TEM images of heat treated SLM 17-4 PH SS are shown in Fig. 6a–d. The aged sampled exhibited incipient dislocation cell structures in martensite lath. Moreover, an abundant precipitation was observed within the cell structure, being most of these precipitates spherical in shape and no coherent with the matrix. Fig. 6b–d shows the dark field, bright-filed and high-resolution images of the precipitates, most of them have a very small size (less than 5 nm) although some aggregates were more than 10 nm in size (Fig. 6b). In addition, no triangular precipitates were observed as reported by Murr et al. in aged SLM 17-4 PH SS [19]. However, the precipitates were also quite homogeneous in size (100–300 nm) as in the work of Murr et al. [19].

As it is well known, the hardening of 17-4 PH SS steel is attributed to copper precipitates in the martensitic matrix. The high density of dislocations provides a high amount of nucleation sites and facilitates diffusion and, therefore, the precipitation of copper. Fig. 7 shows EDS maps for Cu, Fe, Cr, Ni, and Nb confirming that the precipitates are Cu within the martensitic matrix (Fe, Cr, Ni). As stated before, it is expected that these nanoprecipitates increase the hardness of the material with respect to the as-built condition, which is discussed in the next section.

Finally, as observed by Lashgari et al. [44], no carbides were observed. Some large polygonal precipitates have been found such as the one observed in Fig. 8a. Fig. 8b–f shows the EDS maps for Nb, Cr, Ni, Fe and Cu. The results indicated that the polygonal precipitate shown in Fig. 8a is a Nb/Cr-rich nitride, which most likely is originated due to the rapid cooling during the manufacturing process of the SLM and was not dissolved in the solubilised stage of the heat treatment.

3.2. *Micro- and macrohardness*

Macro and microhardness studies were used to see the effect of the manufacturing process and the heat treatment on the mechanical properties of 17-4 PH SS. Fig. 9 shows the variation of macro/microhardness in the as-built condition and after thermal treatment at 1050 °C for 1 h (solubilised) followed by precipitation hardening at 550 °C for 5 h in comparison with wrought steel. As it can be observed in the figure, a good correlation between the results of both tests was obtained indicating a low degree of porosity in the samples. The hardness of wrought specimen is larger than the obtained in the as-built SLM sample as a result of the effect of the heat treatment applied to wrought sample during the manufacturing process. The wrought sample, in the as-produced state, had been subjected to a solubilisation and aged heat treatment with the subsequent Cu-rich precipitation. Moreover, other factors must be considered such as the amount of retained austenite. The XRD spectra of both wrought and as-built sample showed the fcc structure, and that the amount of retained austenite could be higher in the SLM sample due to the gamma effect of nitrogen [51] and might also lead to an additional decrease in hardness. In addition, some previous works have reported that SLM samples are softer than their wrought counterpart [50,52] whereas other authors indicated the opposite [51,53]. In any case, undoubtedly, the type of used powders and the processing parameters can explain these differences. In the present work,

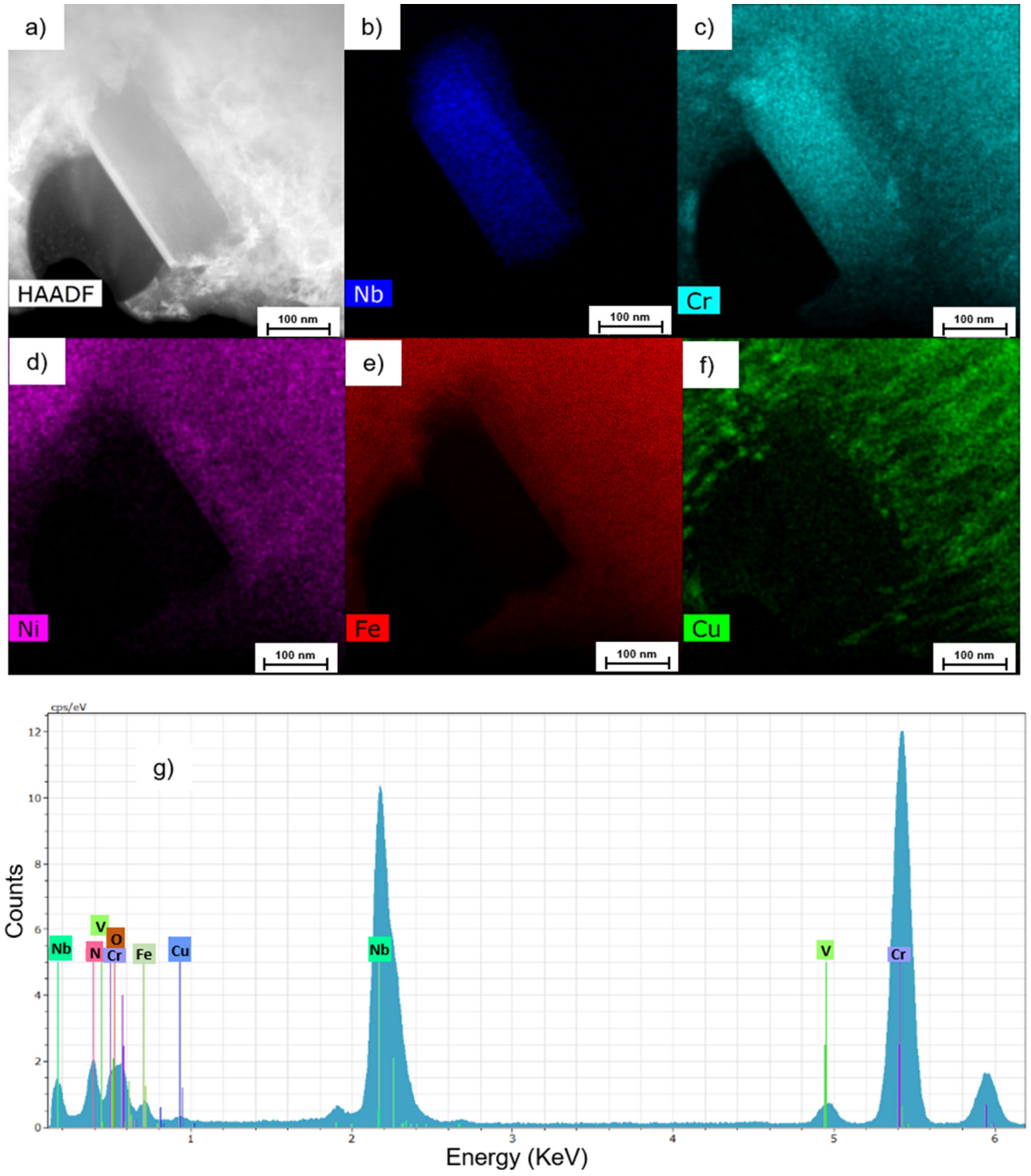

Fig. 8 – Systematic analysis for Nb precipitates. a) Brigh field image, b) X-ray map of Nb, c) X-ray map of Cr, d) X-ray map of Ni, e) X-ray map of Fe, f) X-ray map of Cu and g) X-ray spectrum.

the obtained values of hardness are similar to those reported in the literature and in accordance with the martensitic structure in a 17-4 PH SS, giving lower values of hardness due to the lower amount of carbon in this steel.

The standard deviation value was higher in the as-built SLM samples and can be attributed to the microstructural heterogeneities caused during the additive manufacturing such as dendritic segregation, columnar grains, sub-grain structure, etc. [54].

On the other hand, the evolution of the macro and micro-hardness with the heat treatments can be clearly observed in Fig. 9 and Table 4. The results showed that the solubilised

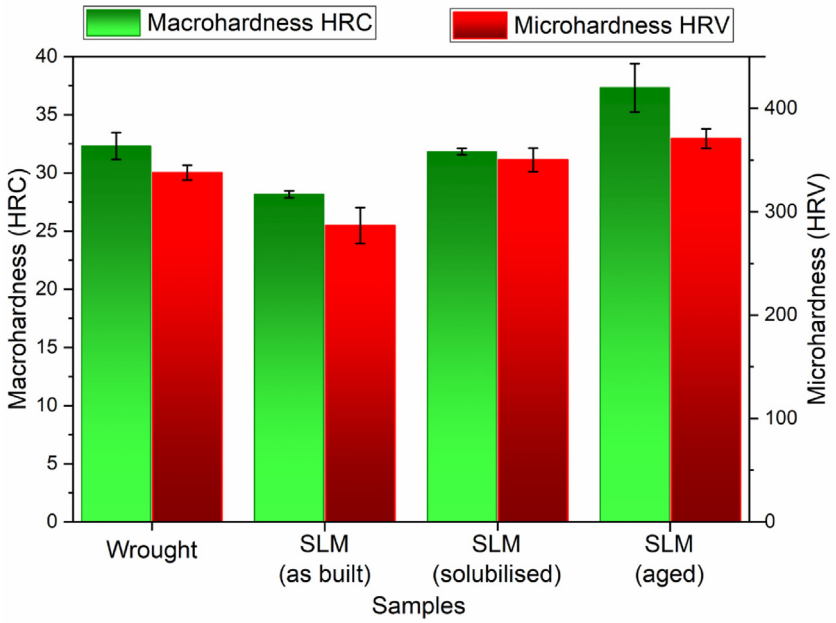

Fig. 9 – Macro and microhardness of the 17-4 PH SS samples.

treatment increased the hardness by 20% in comparison to the as-built sample. This behaviour can be caused by the homogenizing treatment which is responsible for the recrystallization of columnar grains that contribute to increasing the hardness. However, the main cause of this greater increase in the hardness is attributed to the lower volume fraction of austenite which has been observed by XRD although the observed decrease of Cr- and Nb-rich precipitates could also lead to decrease the hardness. These opposite effects can explain the fact that in the literature some studies have reported a decrease in the hardness after the solubilisation treatment with respect to the as-built state [44,55] and other has reported the opposite [56].

Finally, it was found that the micro/microhardness of 17-4 PH SS in aged state increased further with respect to the hardness in the solubilised state, even though an increase in the austenite amount was found by XRD spectra in these aged samples. This increase in hardness is mainly attributed to the increase of Cr and Nb-rich precipitates and also to the formation of nanosized Cu-precipitates [57,58] that can act as obstacles to the movement of dislocations in accordance with the well-known Orowan mechanism [59]. It has also been reported that the high density of dislocations in the martensitic phase of 17-4 PH SS can lead to a faster formation of Cu-rich precipitates due to the dislocation tube diffusion mechanism [60]. This precipitation hardening compensates and overcomes the decrease in the hardness caused by the reverse austenite formed during ageing.

Finally, it can be concluded that the heat treatment has led to values of hardness similar to those obtained in wrought steel, or even higher, due to the predominance of the martensitic structure in the solubilised steel and because of the precipitation hardening in the case of the aged steel.

Table 4 – Macro and microhardness test values.

	Macrohardness (HRC)	Microhardness (HRV)
Wrought	32.3 ± 1.2	337.9 ± 7.3
SLM (as built)	28.2 ± 0.3	286.6 ± 17.5
SLM (solubilised)	31.8 ± 0.3	350.3 ± 11.4
SLM (aged)	37.3 ± 2.1	370.8 ± 9.5

3.3. *Corrosion behaviour*

3.3.1. *Effect of the manufacturing process*

One of the objectives of this article is to analyse the corrosion performance in a biological medium of the 17-4 PH SS parts manufactured by SLM to be compared to their counterparts, conventionally fabricated. For this purpose, three electrochemical testing has been carried out: Open Circuit Potential (OCP), Potentiodynamic Polarization (PDP) and Electrochemical Impedance Spectroscopy (EIS). The corrosion performance of SS is highly dependent on the growth and stability of a chromium oxide passive film which is a function of several parameters: alloy composition, corrosive media, microstructure, etc. [61]. OCP was recorded over time to obtain information about the passive film formation and the corrosion behaviour of the 17-4 PH SS samples.

Moreover, the OCP of as-built 17-4 PH SS, both X–Y plane and X–Z plane, was also analysed to determine the isotropic or anisotropic corrosion behaviour and to be compared to wrought specimen. At first, the wrought sample exhibits a more positive OCP than the SLM sample, decreasing the difference between their OCP values over time and, therefore, SLM samples showed a more stable behaviour over time, Fig. 10a. The SLM X–Z plane sample displayed slightly higher potential than the X–Y plane sample.

The polarization curves showed in Fig. 10b are the usual ones for an unstable passive film, typically exhibited by a

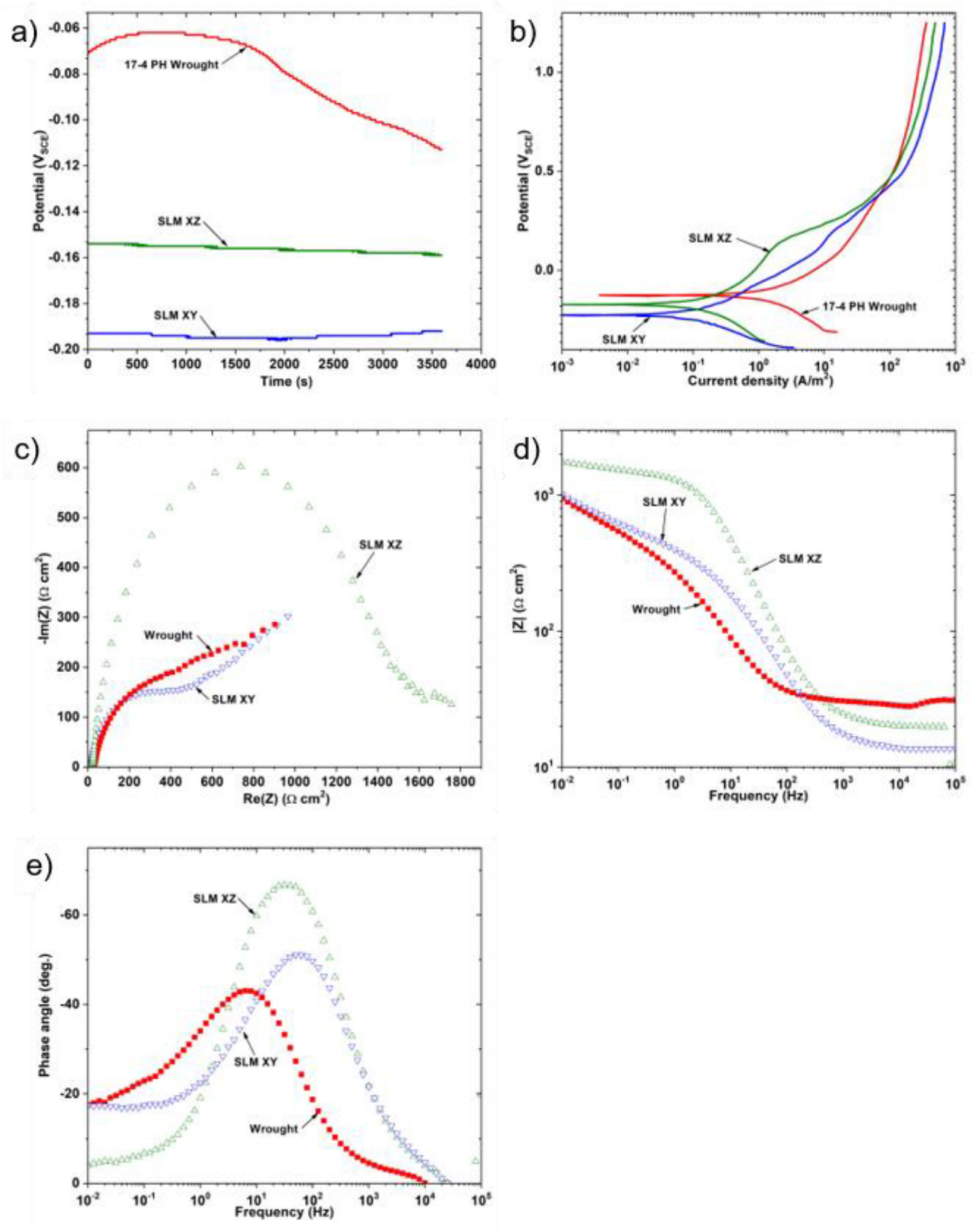

Fig. 10 – Results obtained in the corrosion tests. a) OCP curves, b) Polarization curves, c) Nyquist plot, d) Bode plot (impedance vs frequency) and e) Bode plot (phase vs frequency).

Table 5 – Corrosion parameters obtained from the tests.

Sample	E_{corr} (V)	I_{corr} ($\mu A/cm^2$)	R_p (Ω/cm^2)	E (V)
Wrought	−0.126	25.11	219	–
3D-SLM X–Y	−0.221	2.46	2709	0.178
3D-SLM X–Z	−0.173	8.22	2271	0.125
3D-SLM X–Z (S)	−0.011	0.79	84966	–
3D-SLM X–Z (S + A)	−0.127	1.02	85621	0.092

stainless-steel alloy without a clearly defined passive region [22]. However, this result has been observed in other studies for this material in neutral chloride solution [42,62]. For this reason, it is difficult to establish characteristic corrosion parameters of this material. Nevertheless, the corrosion potential (E_{corr}), corrosion current density (I_{corr}) and polarization resistance (R_p) were extrapolated by Tafel analysis and summarized in Table 5. The E_{corr} value of wrought sample was higher than the obtained for SLM samples which is in good correlation with the OCP results, indicating that the wrought material is more noble than the others. Moreover, the I_{corr} of the SLM X–Z plane is approximately 10 times lower than the I_{corr} of the wrought. This result is quite consistent with previous corrosion rate results in acid chloride [22] and other studies [42,55]. Fig. 10b revealed that both the wrought and SLM alloys exhibited a similar behaviour over the passive range but with a different potential value for the initiation of pitting corrosion. The wrought sample showed a continuous dissolution behaviour but in contrast, SLM samples showed a clear pitting potential and higher current densities. The lower pitting current density exhibited by the wrought alloy suggests that the pitting resistance in that alloy is slightly better than in the SLM samples in PBS environment at high potentials.

EIS measurements have been used to characterize and compare the electrochemical interface between the 17-4 PH SS and the PBS electrolyte for the SLM samples and the wrought sample as reference. The Nyquist plot constructed from EIS data tested is presented in Fig. 10c. The results showed a similar depressed capacitive semicircle in the high frequency region for both the SLM material and the wrought sample. This depressed form is related to the semi-conductive capacitive behaviour of the electrodes and to the non-uniform distribution of the current and the potential as a result of the structural features such as the surface porosity and/or roughness [63], and other surface heterogeneities [64]. The line at low frequencies revealed that the process is controlled by the diffusion phenomena. In general, a larger diameter of the semi-circle is representative of a higher corrosion resistance of the material and, therefore, in this case SLM samples showed a better corrosion behaviour, and SLM X–Z sample exhibited the highest corrosion resistance.

The Bode plots are shown in Fig. 10d and e. The impedance plot reveals that the SLM samples experienced an increase in the impedance module at low-medium frequencies values in comparison with the wrought material and this increase is reduced at high frequencies without practically no distinction between the samples, specially between SLM samples (X–Y plane and X–Z plane).

For all samples, a peak is observed in the phase diagram that is characteristic of a passive behaviour. The phase angle plot provided maximum phase angles of 66°, 52° and 45° for the SLM (X–Z plane and X–Y plane) and wrought samples, respectively. The SLM X–Z plane exhibited a higher phase angle which implies the formation of a more compact passive film on the surface. Considering that the additive manufacturing process is known to promote the formation of pores, elemental segregation, inclusions, carbides and other undesirable phases may increase the probability of a localized corrosion attack, and therefore, it is expected that SLM samples provide a poorer corrosion behaviour than the conventional steel [65]. However, previous studies carried out in acid chloride evidenced that 17-4 PH SS processed by SLM had a better corrosion behaviour its wrought counterpart [22] finding that the low porosity; the low content of oxides and sulphurs; the nitrogen retained in austenite [42], and the fine martensitic microstructure obtained in SLM manufactured samples might explain this better behaviour. In the present work, the electrochemical tests in PBS have shown that the SLM material perpendicular to build direction (X–Y plane) displayed a similar corrosion resistance compared to wrought 17-4 PH SS, but the corrosion behaviour of the SLM material parallel to build direction (X–Z plane) is quite superior. These results agree with those obtained by Stoud et al. [42] in 0.5% NaCl solution. Finally, a recent study shows that the passive film formed on AM SS used for bio applications is more stable with a better barrier compared to the traditional counterparts [66], but in that study a post-built heat treatment has been applied in the specimens.

3.3.2. *Effect of the heat treatment*

The corrosion behaviour of the SLM samples after a heat treatment was study in PBS solution using the same electrochemical tests described in previous paragraphs. The SLM X–Z plane was selected for this comparative study due to their better corrosion behaviour previously described. The samples were tested after the solubilisation -named as (S)- and after the solubilisation and aged -named as (S + A)-.

Fig. 11a shows the open circuit potential curves of the as-built and heat treated 17-4 PH SS samples. The OCP values of the 17-4 PH SS samples are quite different since the OCP of the as-built sample remained stable over time, in contrast, the heat-treated samples showed a different behaviour: OCP of the solubilised sample increases over time and for the S + A sample is the opposite. Finally, the solubilised sample showed the more noble potential, indicating a higher thermodynamic corrosion resistance.

Regarding the results obtained in the anodic polarization measurements, the curves of the heat-treated samples appeared shifted to higher potentials and at lower current densities in comparison with the as-built sample, Fig. 11b. The shape of the solubilised sample scans was similar to those of the wrought sample, a continuous and unstable passivation was observed without a clear pitting potential. The extrapolated corrosion parameters are summarized in Table 6. The E_{corr} value of the solubilised is higher (−0.01V) than that for the as-built sample (−0.17 V) and similar to the solubilised sample (−0.12 V). The corrosion current density of solubilised sample is the lowest (0.39 $\mu A\ cm^{-2}$) and, approximately, 10 times lower than the obtained with the as-built samples, the aging treatment caused a subsequent slight increase in the

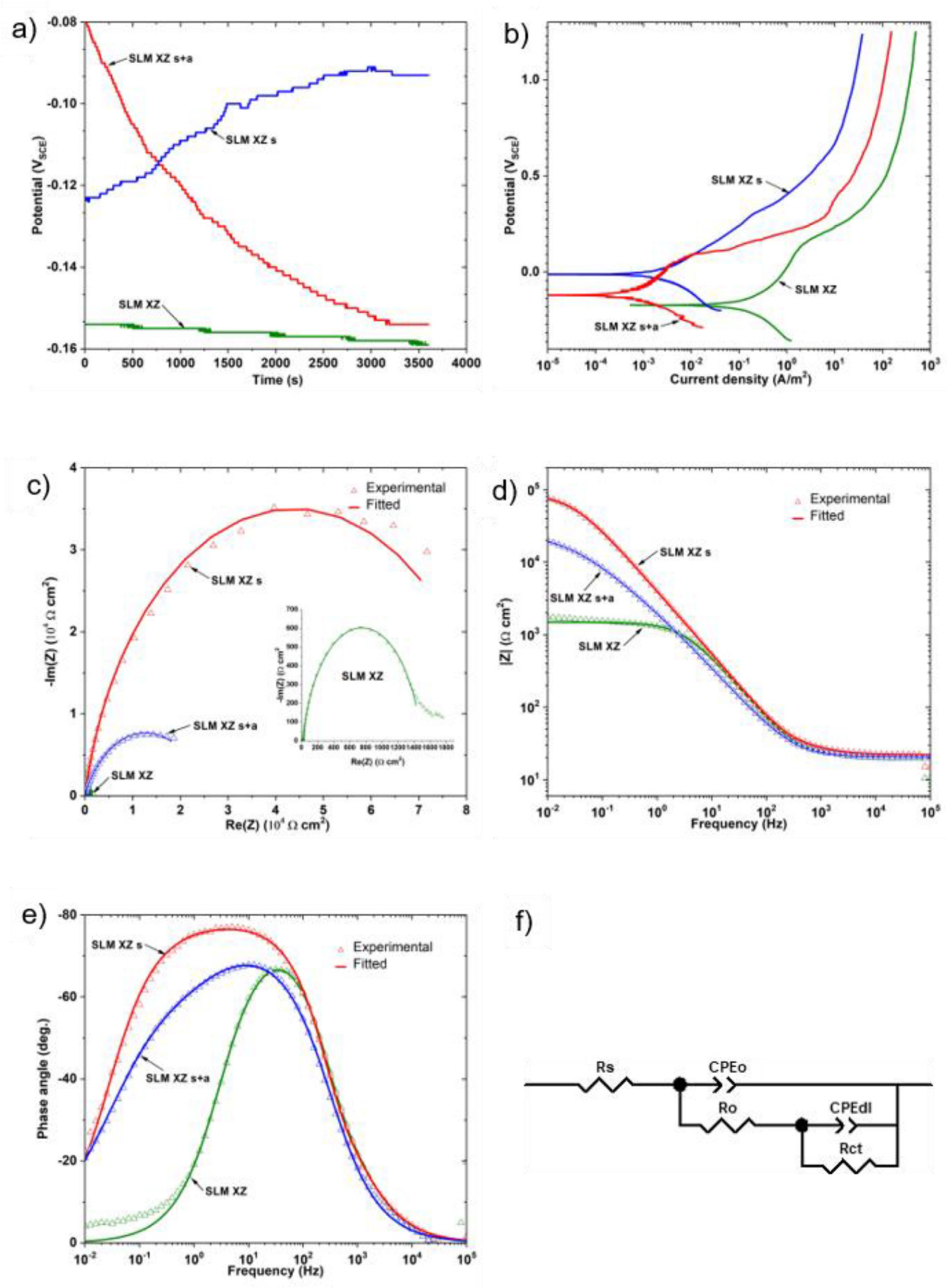

Fig. 11 – Results obtained in the corrosion tests for SLM samples after the heat treatment. a) OCP curves, b) Polarization curves, c) Nyquist plot, d) Bode plot (impedance vs frequency), e) Bode plot (phase vs frequency), f) EIS equivalent circuit.

Table 6 – EIS equivalent circuit parameters of samples.

Sample	R_s (Ω/cm^2)	C_O-C (μF/cm^2)	C_O-n	R_O (Ω/cm^2)	C_{DL}-C (μF/cm^2)	C_{DL}-n	R_2 (kΩ/cm^2)	χ^2 (10^{-4})
3D-SLM X–Z	19.8	50	0.86	64.0	2.8	1	1.4	5
3D-SLM X–Z (S)	22.1	48	0.85	58.8	3.6	1	87.7	6
3D-SLM X–Z (S + A)	20.5	95	0.82	4405	83.9	0.57	21.6	3

current density. The low corrosion current density indicates a low corrosion rate of the post-built heat-treated samples. This result is quite consistent with the results described in the literature [9,67].

The results of impedance spectra measurements shown in Fig. 11c–e evidence important differences between the as-built and heat-treated samples. The Nyquist plots of the heat-treated samples show a large capacitive semi-circle indicating the existence of the passive protective layer on the surface that is the main reason of the high corrosion resistance of the SS. The impedance in Bode plot reveals that the heat-treated samples experienced an increase in impedance module compared to as-built material, especially in the low frequency region (Fig. 11d) and e shows that the phase angle was maximum for the solubilised sample which might be attributable to the formation of a compact thick passive film caused by the heat treatments.

The EIS results were fitted to an equivalent circuit (Fig. 11f) using the CorrView analysis software, the EIS parameters are summarized in Table 6. This circuit model is just one of the several available equivalents circuit and has been proposed by other researchers for 17-4 PH SS [68]. The inserts show the equivalent electrical circuit model where R_s represents the solution resistance and CPE is the constant phase element instead of C capacitance. There are two CPEs, the first is the parallel combination of CPE_o and R_o in the oxide layer impregnated with electrolyte. The electrolyte can penetrate through the pores of the passive layer and cause the metal to dissolve, generating a second time constant. The second relates to the parallel combination of R_{ct} (electron transfer resistance) and CPE_{dl} (double layer CPE). The CPE is considered to explain the impedance properties of this behaviour (when n changes between 0.5 (Warburg) and 1 (ideal capacitor)) and can be calculated from Equation:

$$Z_Q = \left[C(jw)^n\right]^{-1}$$

where C is the capacitance (μF/cm^2), ω is represented the angular frequency (rd/s) and n is the frequency independent parameters that depends on the surface roughness. As shown, R_s, R_o, and R_{ct} are the resistance of the solution, the active areas or the oxide and charge-transfer and CPE_{dl} and CPE_o are the capacity of the double layer and the oxide or active regions, respectively, and W is the Warburg impedance. This model has been successfully used to adjust the impedance spectra of 17-4 PH SS [69,70]. So, the polarization resistance in the electrolyte, R_p (sum of R_o and R_{ct}), is the resistance through the film and across the oxide/electrolyte interface and could be associated to the corrosion resistance.

In comparison with the untreated sample, the solubilised sample showed the highest Rp value which represents the least suppressed loop among the different samples shown in Fig. 11c. On the other hand, the aged sample showed a higher Rp value than the untreated sample but lower than the solubilised one. These results confirm that the solubilised treatment provide a higher corrosion resistance compared to other conditions.

The obtained results demonstrate that the corrosion rate of as-built sample is likely to be higher than those samples

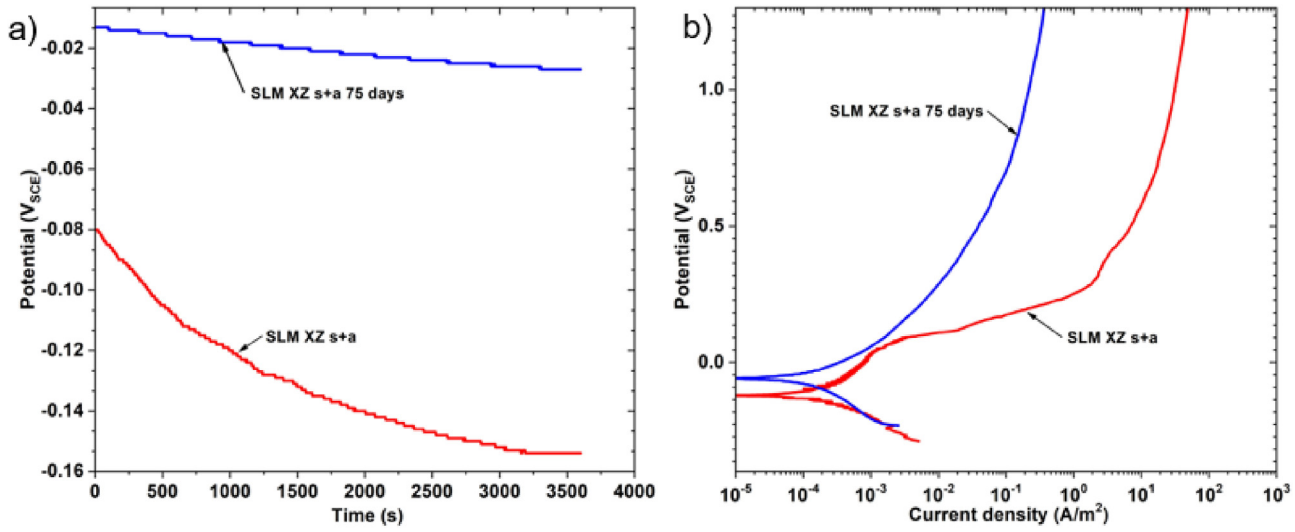

Fig. 12 – Variation exhibited by the SLM sample (solubilised and aged) after 75 days with respect to the initial ones. a) OCP curves and b) Polarization curves.

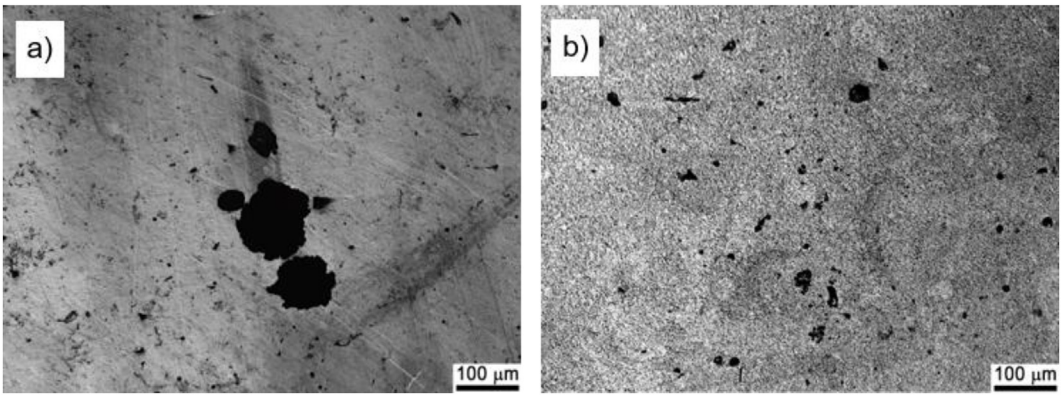

Fig. 13 – Optical micrographs of the surface of the SLM aged samples after the polarization test. a) Samples without immersion, b) Samples with 75 days of immersion.

subjected to heat treatments, and this could be due to that the solubilisation treatment relieves stress of the martensite matrix [71], destroys large solidification grains that grow preferentially along an axis aligned toward the moving heat source and remove the segregation of chromium at the grain boundaries [72]. The morphology and type of precipitates also influence corrosion behaviour. Chromium-rich carbides or nitrides can increase susceptibility to localized corrosion that will degrade the passive layer [73]. The small chromium/niobium-rich precipitates observed in the microstructure of the SLM samples would lead to an overall enhancement in the instability of the passive film, these precipitates disappeared with solubilisation treatment and promoting a better corrosion behaviour. The aged heat treatment promoting a new increase of precipitates, and the lower chromium content on the matrix causes the decrease in corrosion resistance [73]. Moreover, aging heat treatment promote the formation of revert austenite [74] and consequently, galvanic coupling can be formed.

Finally, it can be concluded that a clear improvement of mechanical and corrosion behaviour is observed in the SLM 17-PH SS that could be related with the nitrogen content (0.0829 ± 0.0007%w). Therefore, the higher amount of nitrogen of sintered sample promotes the formation of a nickel and nitrogen rich austenite phase and this enrichment affects the chemical content and crystallinity of the passivation film, improving its pitting corrosion resistance [75]. This retained austenite in the as-built steel could be transformed into martensite by heat treatment with a considerable increase in hardness [76]. In addition, the homogeneous distribution of nitrogen in the retained austenite and the precipitation of NbCN could produce a more stable passive film in heat treatment samples, as reported by Stoudt et al. [75].

Finally, in view of the results, it is expected that for the precipitation-strengthened martensitic SSs (including SLM 17-4 PH), a heat treatment of the as-built steel is required to produce the desired mechanical and corrosion behaviour.

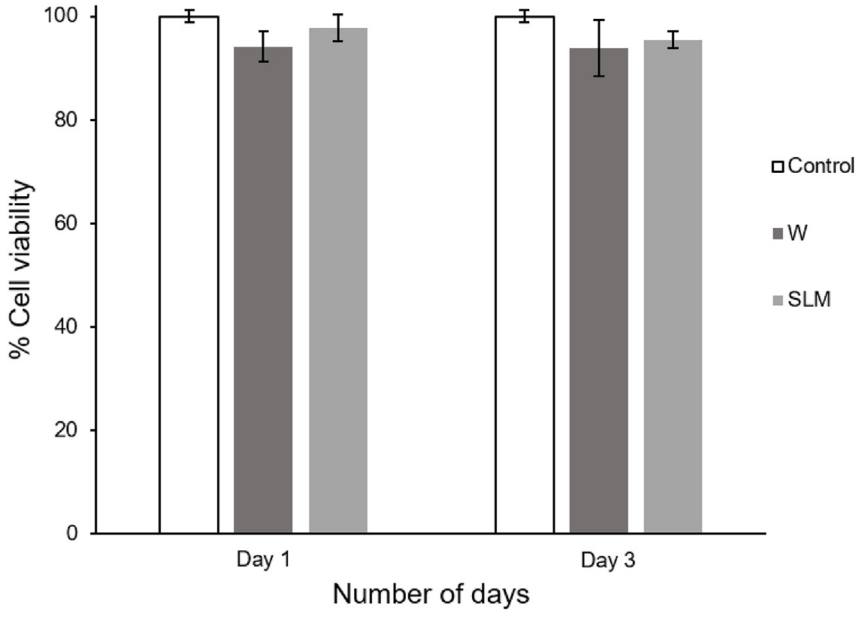

Fig. 14 – Metabolic activity of MC3T3-E1 cells in the presence of W and SLM 17-4 PH SS normalized to the positive control (considered as 100% metabolic activity), after 1 and 3 days of culture.

3.3.3. *Corrosion behaviour after immersion test*

The SLM 17-4 PH heat treated samples that have shown an improved corrosion resistance, as reported before, were immersed during 75 days on PBS solution at 37 °C to determine the effect of the immersion time in passive film. Fig. 12a shows the variation in the OCP values of the SLM sample (solubilised and aged) after 75 days with respect to the initial ones where it is observed a clear shift to more noble values of OCP for the sample after 75 days of immersion, indicating a passive film with better corrosion resistance. The immersion test originated an important change on the shape of the anodic polarization curves. As can be observed in Fig. 12b, the sample experimented a clear improvement in the passive behaviour after the test without pitting potential and with a significant reduction in the current density. Moreover, an increase in the corrosion potential was observed suggesting the formation of a more compact and less unstable passive film. This behaviour is in accordance with previous results in the literature [77] that confirmed the PBS electrolyte helps to stabilize passive film and improves the protection against corrosion.

The optical micrographs of Fig. 13 show the surface of the SLM aged samples after carried out anodic polarization test on the samples without and with 75 days of immersion, respectively. It can be observed that 17-4 PH SS becomes deteriorated by localized corrosion: deep and large pits were observed in samples after the heat treatment (without immersion) while relative smaller pits appeared in the heat-treated samples after immersion. The corrosion sites are more likely initiated from existing isolated residual pores or metallic inclusions, which could cause a discontinuous protective film.

Finally, the determination of the chemical interaction of metallic implants with the body fluids is essential to understand their stability in the body. For bio applications, it is critically important to minimize the risk of released metals from the bulk material. In order to know the quantities of primary metal elements released from the aged SLM 17-4 PH SS samples into the PBS electrolyte after the 75 days of immersion, the concentration of the elements in the liquid was determined by ICP-OES technique. The presence of metals such as Cu, Cr, Fe, Ni and Mo is essential for various biochemical and physiological functions, however, a high amount of these metals in human body can lead to toxicity and risk of carcinogenesis [78]. The concentration obtained for each element after 75 days of immersion was: Fe (52 ± 3 ppb), Cr (31 ± 2 ppb), Ni (76 ± 4 ppb), Cu (46 ± 2 ppb) and Mo (8 ± 1 ppb). The obtained results have been

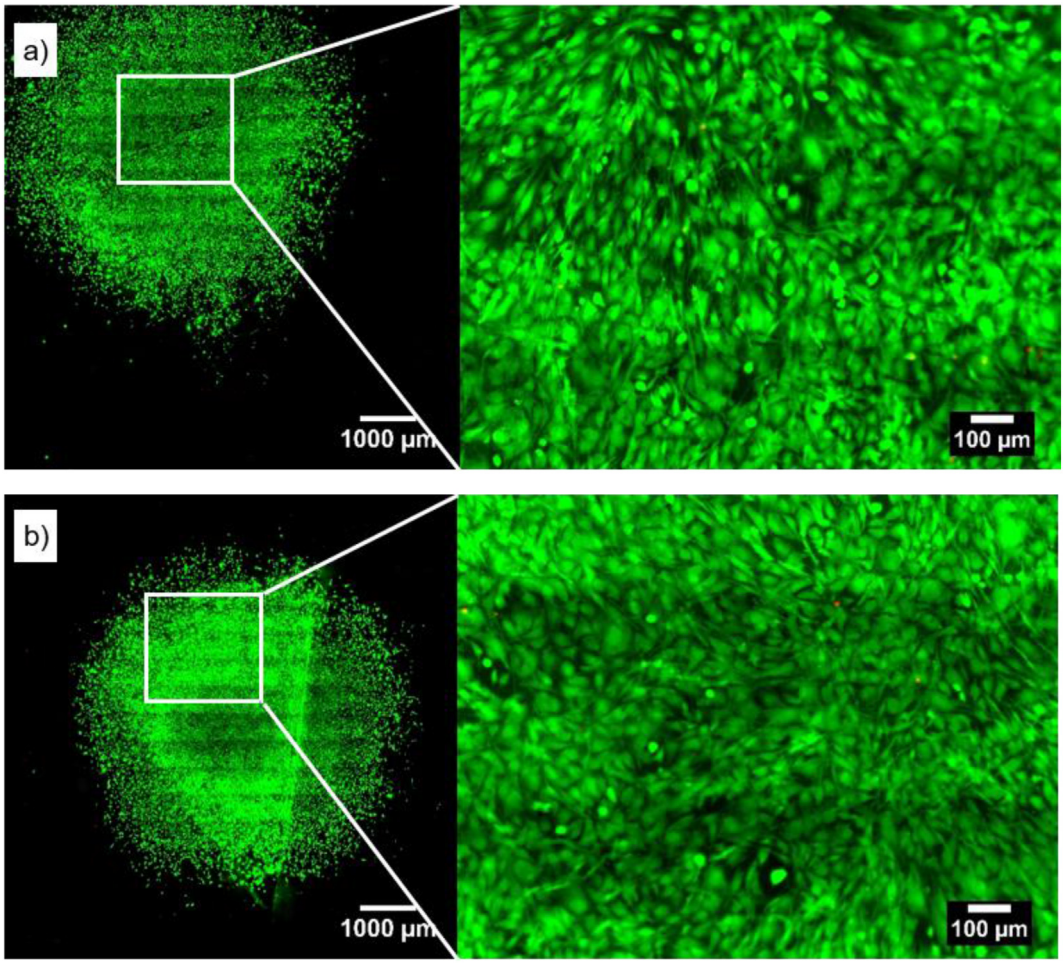

Fig. 15 – LIVE/DEAD assay of MC3T3-E1 preosteoblasts cultured in contact with a) W and b) SLM 17-4 PH surfaces after 3 days. Upper image for each timepoint shows a mosaic of almost the full.

compared with reference levels of these metal ions in human body fluids reported in the literature [79,80]. In view of the results, it can be concluded that the concentration of these ions in the electrolyte is not relevant for human body fluids. This result can be attributed to the resistance of the strong passive film on the 17-4 PH SS after the heat treatment.

3.4. *Cytocompatibility test results*

Cytotoxicity evaluation is a mandatory study for materials aimed to biomedical applications. The effect of manufacturing process conducted in 17-4 PH SS using MC3T3-E1 preosteoblasts cells are shown in Fig. 14. It is possible to observe that the cell viabilities are all larger than 90% after 1 and 3 days of incubation time. Viability values did not decrease with incubation time, therefore these materials do not have a potential cytotoxicological risk on cells. AlamarBlue reduction results show that the presence of manufacturing process does not influence the metabolic activity of MC3T3-E1 cells, since no significant differences were found between the measurements obtained from cells in contact with the metallic surfaces and the positive control after 1 and 3 days of culture. Moreover, the values of % cell viability was slightly higher for SLM 17-4 PH SS, which is probably caused by its higher roughness. Similar results of cell proliferation have been obtained by other authors [81].

The evaluation of cell viability through the LIVE/DEAD assay showed that MC3T3-E1 preosteoblasts in contact with the different metallic surfaces were viable similarly to the positive control. Cells were also found to proliferate over time (Fig. 15), as confirmed by the difference in the number of cells between day 1 and day 3. Results showed a new bioactive layer of cells on the surface of both samples after 3 days of incubation time, which can be attributed to the proliferation, elongation, and well distribution of the cells on the surfaces, exhibiting a good biocompatibility.

4. Conclusions

The present study aims to investigate the influence of heat treatment on the microstructure, hardness, and corrosion resistance in PBS medium of 17-4 PH stainless steel processed by SLM in comparison to the commercial wrought counterparts. The main conclusions of this work are summarized below:

1. Regarding microstructure, wrought steel has a more homogeneous microstructure, while SLM-produced steel is more heterogeneous due to the presence of columnar grains and overlapping melt pools. Post-processing heat treatment provide a uniform and reproducible microstructure in SLM samples and eliminate micro-segregation and reduce the amount of Cr–Nb rich precipitates and retained austenite. The presence of nitrogen in the SLM piece may lead to the formation of retained austenite and possible presence of delta ferrite or martensite.
2. The hardness of wrought sample is higher than that of as-built SLM sample, but post-processing heat treatment result in similar or higher hardness values due to the predominance of the martensitic structure and precipitation hardening in solubilised and aged steel.
3. Regarding corrosion, post-processed SLM samples showed a more stable behaviour over time than wrought samples in three electrochemical tests. Tests also showed that solubilised samples have better corrosion performance than solubilised and aged samples.
4. In addition, the concentrations of primary metallic elements released from aged SLM 17-4 PH SS samples to PBS electrolyte after 75 days of immersion are not relevant to human body fluids. Results indicating that such material is likely to be used as a biomaterial.

In summary, it can be said that 17-4 PH SS processed by conventional manufacturing (wrought) and additive manu facturing (SLM) present significant differences in microstructure and mechanical and corrosion properties, aspects that improve with the application of heat treatment to such steel.

Declaration of competing interest

The authors declare that they have no known competing financial interests or personal relationships that could have appeared to influence the work reported in this paper.

Acknowledgments

This work was supported by MICINN-FEDER (PID2021-122365OB-I00), «Infraestructuras Red de Castilla y Leon (INFRARED)» and JCyL Consejería de Educación - FEDER (VA275P18).

REFERENCES

[1] Wu Y, Lu Y, Zhao M, Bosiakov S, Li L. A critical review of additive manufacturing techniques and associated biomaterials used in bone tissue engineering. Polym 2022;14:2117. https://doi.org/10.3390/POLYM14102117.
[2] Chen Q, Thouas GA. Metallic implant biomaterials. Mater Sci Eng R Rep 2015;87:1–57. https://doi.org/10.1016/J.MSER.2014.10.001.
[3] Tipan N, Pandey A, Mishra P. Selection and preparation strategies of Mg-alloys and other biodegradable materials for orthopaedic applications: a review. Mater Today Commun 2022;31:103658. https://doi.org/10.1016/j.mtcomm.2022.103658.
[4] Wang W, Han J, Yang X, Li M, Wan P, Tan L, et al. Novel biocompatible magnesium alloys design with nutrient alloying elements Si, Ca and Sr: structure and properties characterization. Mater Sci Eng B 2016;214:26–36. https://doi.org/10.1016/j.mseb.2016.08.005.
[5] Tian L, Tang N, Ngai T, Wu C, Ruan Y, Huang L, et al. Hybrid fracture fixation systems developed for orthopaedic applications: a general review. J Orthop Transl 2019;16:1–13. https://doi.org/10.1016/j.jot.2018.06.006.
[6] Carneiro L, Jalalahmadi B, Ashtekar A, Jiang Y. Cyclic deformation and fatigue behavior of additively manufactured 17–4 PH stainless steel. Int J Fatig

2019;123:22–30. https://doi.org/10.1016/j.ijfatigue.2019.02.006.
[7] Nouri A, Rohani Shirvan A, Li Y, Wen C. Additive manufacturing of metallic and polymeric load-bearing biomaterials using laser powder bed fusion: a review. J Mater Sci Technol 2021;94:196–215. https://doi.org/10.1016/j.jmst.2021.03.058.
[8] Sanguedolce M, Zekonyte J, Alfano M. Wear of 17-4 PH stainless steel patterned surfaces fabricated using selective laser melting. Appl Sci 2021;11:9317. https://doi.org/10.3390/app11199317.
[9] Kosasang O, Wongkaewmoon M, Chumphoongphan S. Effect of aging heat treatment on corrosion behavior and corrosion kinetics of 17-4PH stainless steel in artificial saliva. Sains Malays 2021;50:849–58. https://doi.org/10.17576/jsm-2021-5003-25.
[10] Wu Y, German RM, Blaine D, Marx B, Schlaefer C. Effects of residual carbon content on sintering shrinkage, microstructure and mechanical properties of injection molded 17-4 PH stainless Steel. J Mater Sci 2002;37:3573–83. https://doi.org/10.1023/A:1016532418920.
[11] Shen S, Li X, Zhang P, Nana Y, Yangb G, Song X. Effect of solution-treated temperature on hydrogen embrittlement of 17-4 PH stainless Steel. Mater Sci Eng, A 2017;703:413–21. https://doi.org/10.1016/J.MSEA.2017.06.078.
[12] Abe Y, Kurose T, Santos MVA, Kanaya Y, Ishigami A, Tanaka S, et al. Effect of layer directions on internal structures and tensile properties of 17-4PH stainless steel parts fabricated by fused deposition of metals. Materials 2021;14:243. https://doi.org/10.3390/ma14020243.
[13] Mutlu I, Oktay E. Influence of fluoride content of artificial saliva on metal release from 17-4 PH stainless steel foam for dental implant applications. J Mater Sci Technol 2013;29:582–8. https://doi.org/10.1016/j.jmst.2013.03.006.
[14] Mutlu I, Oktay E. Biocompatibility of 17-4 PH stainless steel foam for implant applications. Bio Med Mater Eng 2011;21:223–33. https://doi.org/10.3233/BME-2011-0671.
[15] Dehghan-Manshadi A, Yu P, Dargusch M, StJohn D, Qian M. Metal injection moulding of surgical tools, biomaterials and medical devices: a review. Powder Technol 2020;364:189–204. https://doi.org/10.1016/j.powtec.2020.01.073.
[16] Gulsoy HO, Pazarlioglu S, Gulsoy N, Gundede B, Mutlu O. Effect of Zr, Nb and Ti addition on injection molded 316L stainless steel for bio-applications: mechanical, electrochemical and biocompatibility properties. J Mech Behav Biomed Mater 2015;51:215–24. https://doi.org/10.1016/J.JMBBM.2015.07.016.
[17] Ji CH, Loh NH, Khor KA, Tor SB. Sintering study of 316L stainless steel metal injection molding parts using Taguchi method: final density. Mater Sci Eng, A 2001;311:74–82. https://doi.org/10.1016/S0921-5093(01)00942-X.
[18] Li Y, Li L, Khalil KA. Effect of powder loading on metal injection molding stainless steels. J Mater Process Technol 2007;183:432–9. https://doi.org/10.1016/j.jmatprotec.2006.10.039.
[19] Murr LE, Martinez E, Amato KN, Gaytan SM, Hernandez J, Ramirez DA, et al. Fabrication of metal and alloy components by additive manufacturing: examples of 3D materials science. J Mater Res Technol 2012;1:42–54. https://doi.org/10.1016/S2238-7854(12)70009-1.
[20] Germaini MM, Belhabib S, Guessasma S, Deterre R, Corre P, Weiss P. Additive manufacturing of biomaterials for bone tissue engineering – a critical review of the state of the art and new concepts. Prog Mater Sci 2022;130:100963. https://doi.org/10.1016/J.PMATSCI.2022.100963.
[21] Hong MH, Hanawa T, Song SH, Min BK, Kwon TY. Enhanced biocompatibility of a Ni–Cr alloy prepared by selective laser melting: a preliminary in vitro study. J Mater Res Technol 2019;8:1587–92. https://doi.org/10.1016/J.JMRT.2018.08.004.
[22] Garcia-Cabezon C, Castro-Sastre MA, Fernandez-Abia AI, Rodriguez-Mendez ML, Martin-Pedrosa F. Microstructure–hardness–corrosion performance of 17–4 precipitation hardening stainless steels processed by selective laser melting in comparison with commercial alloy. Met Mater Int 2022;28:2652–67. https://doi.org/10.1007/S12540-021-01155-8/TABLES/5.
[23] Prasetyadi T, Irawan B, Purwanegara MK, Suharno B, Supriadi S. Cytotoxicity of ions released from 17-4 precipitation hardening stainless steel orthodontic brackets in artificial saliva. Int J Appl Pharm 2017;9:71–3. https://doi.org/10.22159/ijap.2017.v9s2.17.
[24] Lashgari HR, Xue Y, Onggowarsito C, Kong C, Li S. Microstructure, tribological properties and corrosion behaviour of additively manufactured 17-4PH stainless steel: effects of scanning pattern, build orientation, and single vs. double scan. Mater Today Commun 2020;25:101535. https://doi.org/10.1016/j.mtcomm.2020.101535.
[25] Leo P, Cabibbo M, Del Prete A, Giganto S, Martínez-Pellitero S, Barreiro J. Laser defocusing effect on the microstructure and defects of 17-4PH parts additively manufactured by SLM at a low energy input. Metals 2021;11:588. https://doi.org/10.3390/met11040588.
[26] Giganto S, Martínez-Pellitero S, Barreiro J, Leo P, Castro-Sastre MA. Impact of the laser scanning strategy on the quality of 17-4PH stainless steel parts manufactured by selective laser melting. J Mater Res Technol 2022;20:2734–47. https://doi.org/10.1016/j.jmrt.2022.08.040.
[27] Shrestha R, Shamsaei N, Seifi M, Phan N. An investigation into specimen property to part performance relationships for laser beam powder bed fusion additive manufacturing. Addit Manuf 2019;29:100807. https://doi.org/10.1016/j.addma.2019.100807.
[28] Karaminezhaad M, Sharafi S, Dalili K. Effect of molybdenum on SCC of 17-4PH stainless steel under different aging conditions in chloride solutions. J Mater Sci 2006;41:3329–33. https://doi.org/10.1007/S10853-005-5416-8.
[29] Khatak Br HS. Corrosion of austenitic stainless steels. 1st. Woodhead P; 2022.
[30] Alnajjar M, Christien F, Bosch C, Wolski K. A comparative study of microstructure and hydrogen embrittlement of selective laser melted and wrought 17–4 PH stainless steel. Mater Sci Eng, A 2020;785:139363. https://doi.org/10.1016/J.MSEA.2020.139363.
[31] Gibson I, Rosen D, Stucker B. Additive manufacturing technologies. 2nd.ed. New York: Springer; 2014. https://doi.org/10.1007/978-1-4939-2113-3.
[32] Murr LE, Martinez E, Hernandez J, Collins S, Amato KN, Gaytan SM, et al. Microstructures and properties of 17-4 PH stainless steel fabricated by selective laser melting. J Mater Res Technol 2012;1:167–77. https://doi.org/10.1016/S2238-7854(12)70029-7.
[33] Yang KT, Kim MK, Kim D, Suhr J. Investigation of laser powder bed fusion manufacturing and post-processing for surface quality of as-built 17-4PH stainless steel. Surf Coating Technol 2021;422:127492. https://doi.org/10.1016/J.SURFCOAT.2021.127492.
[34] Winters GL, Nutt MJ. Stainless steels for medical and surgical applications. ASTM International; 2002.
[35] Balamurugan A, Rajeswari S, Balossier G, Rebelo AHS, Ferreira JMF. Corrosion aspects of metallic implants — an overview. Mater Corros 2008;59:855–69. https://doi.org/10.1002/MACO.200804173.
[36] Sabooni S, Chabok A, Feng SC, Blaauw H, Pijper TC, Yang HJ, et al. Laser powder bed fusion of 17–4 PH stainless steel: a comparative study on the effect of heat treatment on the

microstructure evolution and mechanical properties. Addit Manuf 2021;46:102176. https://doi.org/10.1016/J.ADDMA.2021.102176.
[37] Cheruvathur S, Lass EA, Campbell CE. Additive manufacturing of 17-4 PH stainless steel: post-processing heat treatment to achieve uniform reproducible microstructure. JOM (J Occup Med) 2016;68:930–42. https://doi.org/10.1007/S11837-015-1754-4.
[38] Asri RIM, Harun WSW, Samykano M, Lah NAC, Ghani SAC, Tarlochan F, et al. Corrosion and surface modification on biocompatible metals: a review. Mater Sci Eng C 2017;77:1261–74. https://doi.org/10.1016/J.MSEC.2017.04.102.
[39] Kaur S, Sharma S, Bala N. A comparative study of corrosion resistance of biocompatible coating on titanium alloy and stainless steel. Mater Chem Phys 2019;238:121923. https://doi.org/10.1016/J.MATCHEMPHYS.2019.121923.
[40] ASTM G-5–87. Standard reference test method for making potentiostatic and potentiodynamic anodic polarization measurements. ASTM International; 1993.
[41] ISO 10993-5:2009. Biological evaluation of medical devices - Part 5: tests for in vitro cytotoxicity. ISO; 2009.
[42] Stoudt MR, Ricker RE, Lass EA, Levine LE. Influence of postbuild microstructure on the electrochemical behavior of additively manufactured 17-4 PH stainless steel. JOM (J Occup Med) 2017;69. https://doi.org/10.1007/s11837-016-2237-y.
[43] Smith WF. Structure and properties of engineering alloys. 1st. McGraw-Hill; 1981.
[44] Lashgari HR, Kong C, Adabifiroozjaei E, Li S. Microstructure, post thermal treatment response, and tribological properties of 3D printed 17-4 PH stainless steel. Wear 2020:456–7. https://doi.org/10.1016/j.wear.2020.203367.
[45] Alnajjar M, Christien F, Barnier V, Bosch C, Wolski K, Fortes AD, et al. Influence of microstructure and manganese sulfides on corrosion resistance of selective laser melted 17-4 PH stainless steel in acidic chloride medium. Corrosion Sci 2020;168. https://doi.org/10.1016/j.corsci.2020.108585.
[46] Lippold JC, Kotecki DJ. Welding metallurgy and weldability of stainless steels. Wiley; 2005.
[47] Song YY, Li XY, Rong LJ, Ping DH, Yin FX, Li YY. Formation of the reversed austenite during intercritical tempering in a Fe–13%Cr–4%Ni–Mo martensitic stainless steel. Mater Lett 2010;64:1411–4. https://doi.org/10.1016/j.matlet.2010.03.021.
[48] LeBrun T, Nakamoto T, Horikawa K, Kobayashi H. Effect of retained austenite on subsequent thermal processing and resultant mechanical properties of selective laser melted 17–4 PH stainless steel. Mater Des 2015;81:44–53. https://doi.org/10.1016/J.MATDES.2015.05.026.
[49] Viswanathan UK, Banerjee S, Krishnan R. Effects of aging on the microstructure of 17-4 PH stainless steel. Mater Sci Eng, A 1988;104:181–9. https://doi.org/10.1016/0025-5416(88)90420-X.
[50] Kc S, Nezhadfar PD, Phillips C, Kennedy MS, Shamsaei N, Jackson RL. Tribological behavior of 17–4 PH stainless steel fabricated by traditional manufacturing and laser-based additive manufacturing methods. Wear 2019;440–441:203100. https://doi.org/10.1016/J.WEAR.2019.203100.
[51] Yadollahi A, Shamsaei N, Thompson SM, Elwany A, Bian L. Effects of building orientation and heat treatment on fatigue behavior of selective laser melted 17-4 PH stainless steel. Int J Fatig 2017;94:218–35. https://doi.org/10.1016/j.ijfatigue.2016.03.014.
[52] Sarkar S, Mukherjee S, Kumar CS, Kumar Nath A. Effects of heat treatment on microstructure, mechanical and corrosion properties of 15-5 PH stainless steel parts built by selective laser melting process. J Manuf Process 2020;50:279–94. https://doi.org/10.1016/J.JMAPRO.2019.12.048.
[53] Guo Z, Kindt JT. Partitioning of size-mismatched impurities to grain boundaries in 2d solid hard-sphere monolayers. Langmuir 2018;34:12947–56. https://doi.org/10.1021/ACS.LANGMUIR.8B02633/SUPPL_FILE/LA8B02633_SI_001.AVI.
[54] Yusuf SM, Gao N. Influence of energy density on metallurgy and properties in metal additive manufacturing. Mater Sci Technol 2017;33:1269–89. https://doi.org/10.1080/02670836.2017.1289444.
[55] Mathoho I, Akinlabi ET, Arthur N, Tlotleng M. Impact of DED process parameters on the metallurgical characteristics of 17-4 PH SS deposited using DED. CIRP J Manuf Sci Technol 2020;31:450–8. https://doi.org/10.1016/J.CIRPJ.2020.07.007.
[56] Mahmoudi M, Elwany A, Yadollahi A, Thompson SM, Bian L, Shamsaei N. Mechanical properties and microstructural characterization of selective laser melted 17-4 PH stainless steel. Rapid Prototyp J 2017;23:280–94. https://doi.org/10.1108/RPJ-12-2015-0192.
[57] Wang L, Dong C, Man C, Kong D, Xiao K, Li X. Enhancing the corrosion resistance of selective laser melted 15-5PH martensite stainless steel via heat treatment. Corrosion Sci 2020;166:108427. https://doi.org/10.1016/J.CORSCI.2019.108427.
[58] Kimura H. Precipitation behavior and 2-step aging of 17-4PH stainless steel. Tetsu-To-Hagane/Journal Iron Steel Inst Japan 2000;86:343–8. https://doi.org/10.2355/TETSUTOHAGANE1955.86.5_343.
[59] Ferguson JB, Schultz BF, Venugopalan D, Lopez HF, Rohatgi PK, Cho K, et al. On the superposition of strengthening mechanisms in dispersion strengthened alloys and metal-matrix nanocomposites: considerations of stress and energy. Met Mater Int 2014;20:375–88. https://doi.org/10.1007/S12540-014-2017-6/METRICS.
[60] Yeli G, Auger MA, Wilford K, Smith GDW, Bagot PAJ, Moody MP. Sequential nucleation of phases in a 17-4PH steel: microstructural characterisation and mechanical properties. Acta Mater 2017;125:38–49. https://doi.org/10.1016/J.ACTAMAT.2016.11.052.
[61] Fattah-alhosseini A, Golozar MA, Saatchi A, Raeissi K. Effect of solution concentration on semiconducting properties of passive films formed on austenitic stainless steels. Corrosion Sci 2010;52:205–9. https://doi.org/10.1016/J.CORSCI.2009.09.003.
[62] Forcellese P, Mancia T, Simoncini M, Bellezze T. Investigation on corrosion resistance properties of 17-4 PH bound metal deposition as-sintered specimens with different build-up orientations. Met 2022;12:588. https://doi.org/10.3390/MET12040588.
[63] Pajkossy T. Impedance spectroscopy at interfaces of metals and aqueous solutions — surface roughness, CPE and related issues. Solid State Ionics 2005;176:1997–2003. https://doi.org/10.1016/J.SSI.2004.06.023.
[64] Lakatos-Varsányi M, Furko M, Pozman T. Electrochemical impedance spectroscopy study on silver coated metallic implants. Electrochim Acta 2011;56:7787–95. https://doi.org/10.1016/J.ELECTACTA.2011.01.072.
[65] Hemmasian Ettefagh A, Guo S, Raush J. Corrosion performance of additively manufactured stainless steel parts: a review. Addit Manuf 2021;37:101689. https://doi.org/10.1016/J.ADDMA.2020.101689.
[66] Lodhi MJK, Deen KM, Greenlee-Wacker MC, Haider W. Additively manufactured 316L stainless steel with improved corrosion resistance and biological response for biomedical applications. Addit Manuf 2019;27:8–19. https://doi.org/10.1016/j.addma.2019.02.005.
[67] Pan L, Kwok CT, Niu B, Huang X, Cao Y, Zou X, et al. Enhancement in hardness and corrosion resistance of directed energy deposited 17–4 PH martensitic stainless

steel via heat treatment. J Mater Res Technol 2023;23:1296–311. https://doi.org/10.1016/J.JMRT.2023.01.114.
[68] Bakhshandeh HR, Allahkaram SR, Zabihi AH. An investigation on cavitation-corrosion behavior of Ni/β-SiC nanocomposite coatings under ultrasonic field. Ultrason Sonochem 2019;56:229–39. https://doi.org/10.1016/J.ULTSONCH.2019.04.022.
[69] Al-Mamun NS, Mairaj Deen K, Haider W, Asselin E, Shabib I. Corrosion behavior and biocompatibility of additively manufactured 316L stainless steel in a physiological environment: the effect of citrate ions. Addit Manuf 2020;34:101237. https://doi.org/10.1016/J.ADDMA.2020.101237.
[70] Karthik D, Swaroop S. Electrochemical stability of laser shock peened 17-4 PH stainless steel. Opt Laser Technol 2019;120:105727. https://doi.org/10.1016/J.OPTLASTEC.2019.105727.
[71] Mudali UK, Bhaduri AK, Gnanamoorthy JB. Localised corrosion behaviour of 17–4 PH stainless steel. Mater Sci Technol 2013;6:475–81. https://doi.org/10.1179/MST.1990.6.5.475.
[72] Ziewiec A, Zielińska-Lipiec A, Tasak E. Microstructure of welded joints of X5CrNiCuNb 16-4 (17-4 PH) martensitic stainlees steel after heat treatment. Arch Metall Mater 2014;59:965–70. https://doi.org/10.2478/AMM-2014-0162.
[73] Stoudt MR, Campbell CE, Ricker RE. Examining the relationship between post-build microstructure and the corrosion resistance of additively manufactured 17-4PH stainless steel. Materialia 2022;22:101435. https://doi.org/10.1016/J.MTLA.2022.101435.
[74] Murayama M, Katayama Y, Hono K. Microstructural evolution in a 17-4 PH stainless steel after aging at 400 °C. Metall Mater Trans A Phys Metall Mater Sci 1999;30:345–53. https://doi.org/10.1007/S11661-999-0323-2/METRICS.
[75] Wang L, Dong C, Kong D, Man C, Liang J, Wang C, et al. Effect of manufacturing parameters on the mechanical and corrosion behavior of selective laser-melted 15-5PH stainless steel. Steel Res Int 2020;91:1900447. https://doi.org/10.1002/SRIN.201900447.
[76] Lee JR, Lee MS, Chae H, Lee SY, Na T, Kim WS, et al. Effects of building direction and heat treatment on the local mechanical properties of direct metal laser sintered 15-5 PH stainless steel. Mater Char 2020;167:110468. https://doi.org/10.1016/J.MATCHAR.2020.110468.
[77] Barroux A, Duguet T, Ducommun N, Nivet E, Delgado J, Laffont L, et al. Combined XPS/TEM study of the chemical composition and structure of the passive film formed on additive manufactured 17-4PH stainless steel. Surface Interfac 2021;22:100874. https://doi.org/10.1016/J.SURFIN.2020.100874.
[78] Tchounwou PB, Yedjou CG, Patlolla AK, Sutton DJ. Heavy metal toxicity and the environment. In: Luch A, editor. Molecular, clinical and environmental toxicology. Experientia supplementum, 101. Basel: Springer; 2012. https://doi.org/10.1007/978-3-7643-8340-4_6.
[79] Sargeant A, Goswami T. Hip implants: paper V. Physiological effects. Mater Des 2006;27:287–307. https://doi.org/10.1016/J.MATDES.2004.10.028.
[80] Okazaki Y, Gotoh E. Metal release from stainless steel, Co–Cr–Mo–Ni–Fe and Ni–Ti alloys in vascular implants. Corrosion Sci 2008;50:3429–38. https://doi.org/10.1016/J.CORSCI.2008.09.
[81] Mutlu I, Oktay E. Biocompatibility of 17-4 PH stainless steel foam for implant applications. Bio Med Mater Eng 2011;21:223–33. https://doi.org/10.3233/BME-2011-06.